Monthly Notices of the ROYAL ASTRONOMICAL SOCIETY

MNRAS **521,** 6247–6265 (2023) https://doi.org/10.1093/mnras/stad1001
Advance Access publication 2023 April 05

Comparison of solar activity proxies: eigenvectors versus averaged sunspot numbers

V. V. Zharkova,[1,2]★ I. Vasilieva,[2,3]★ E. Popova[4]★ and S. J. Shepherd[5]

[1]*Department of MPEE, University of Northumbria, Newcastle upon Tyne, NE1 8ST ZVS RE, UK*
[2]*ZVS Research Enterprise Ltd, London, EC1V 2NX, UK*
[3]*Department of Solar Physics, Main Astronomical Observatory, Kyiv, 030143, Ukraine*
[4]*Centro de Investigación en Astronomía, Universidad Bernardo O'Higgins, Santiago, General Gana 1760, Chile*
[5]*PRIMAL Research Group, Sorbonne Universite, Paris 75006, France*

Accepted 2023 March 30. Received 2023 March 30; in original form 2022 August 22

ABSTRACT

We explore the links between the averaged sunspot numbers (SSN) and a modulus summary curve (MSC) of two largest eigenvectors of the solar background magnetic field (SBMF) derived from principal component analysis. MSC has rather close correspondence with the whole set of SSN revealing close cycle timings, duration, and maxima times for the cycles 12–24, 6, 7, and −4, −3, while for a few cycles in the mid-18th and mid-19th centuries there are discrepancies in the maximum amplitudes, durations, and times of the maxima. Possible reasons of these discrepancies related to uncertainties in the SSN observations in the 18th–19th centuries, in MSC definition and the different solar activity entities they represent: toroidal (SSN) and poloidal (MSC) magnetic fields, are discussed. Wavelet and Fourier spectral analysis of SSN and MSC series reveal within 95 per cent confidence levels the same prominent period of 10.7 yr, whereas SSN series show a period of 101 yr and MSC of 342 yr close to or above 95 per cent red-noise level. The correlation coefficients between SSN and MSC series vary from 0.25 for the whole SSN data set (from 1700), to 0.56 for the data sets from 1860, to 0.67 for the data sets from 1900 when all SSN restorations agree. These SSN and MSC data sets are confirmed to be closely but not identically related representing the solar activity in different entities of solar dynamo. Use of the summary curve and MSC of eigenvectors of SBMF can provide additional information to SSN for better understanding of solar activity.

Key words: dynamo – methods: data analysis – methods: statistical – Sun: interior – Sun: magnetic fields – Sun: sunspots.

1 INTRODUCTION

Solar activity is a fundamental process of generation radiation, energetic particles and waves affecting the Earth and other planets, the climate, and human life. The points how sunspot activity varies in time and how it is linked to magnetic activity are very important issues investigated by many researchers. For the past two centuries, a solar cycle was defined through sunspot numbers and this solar activity index was also used for prediction of the future solar activity while testing mechanisms of the solar dynamo providing conversion and transport of solar magnetic fields from the solar interior to its surface. The dynamo models operate with poloidal and toroidal magnetic fields (Parker 1955), with the first one being the solar background magnetic field (SBMF), and the second one being the magnetic field of magnetic loops in active regions, which are embedded into the solar surface, whose roots look like sunspots.

Sunspots were actively studied across various cultures and geographies of the Earth from visual observations before the invention of a telescope and from telescopic monitoring of the Sun after; although, these observations were affected by observational gaps and unquantified uncertainties (Schwabe 1843; Wolf 1850a; Hoyt & Schatten 1998b; Soon & Yaskell 2003; Arlt 2008; Kane 2008; Arlt 2009; Ogurtsov 2013; Clette et al. 2014; Arlt et al. 2016; Zito 2016; Chatzistergos et al. 2017; Hayakawa et al. 2017; Tamazawa et al. 2017; Willamo, Usoskin & Kovaltsov 2017; Neuhäuser, Arlt & Richter 2018; Muñoz-Jaramillo & Vaquero 2019; Arlt & Vaquero 2020; Carrasco, Gallego & Vaquero 2020; Simpson 2020; Carrasco et al. 2021; Hayakawa et al. 2021; Vokhmyanin, Arlt & Zolotova 2021).

For the past 400 yr and even longer than 1000 yr, if Chinese observations are included, sunspots were observed with different level of regularity. In the middle of 19th century, a few experienced observers discovered that dark spots on the sun, sunspots, appear rather periodically with maxima and minima occurring within every 11 yr (Schwabe 1843; Wolf 1850a, b). Based on this periodicity, the first index of solar activity was expressed with monthly sunspot numbers, or Wolf's number W, averaged from many observatories (Wolf 1850a, b). For nearly 300 yr relative Solar sunspot number (SSN) are still used (http://www.sidc.be/silso/home) as the solar activity index.

In addition to SSN, the group sunspot number (GSN) were introduced Hoyt & Schatten (1998a, b), in order to repair a deficiency in observing small sunspots making this index, the resulting GSN, compatible with the SSN. Other authors tried to identify the solar activity nature with underlying solar magnetism giving the full cycle

★ E-mail: valentina.zharkova@northumbria.ac.uk (VVZ); vasil@mao.kiev.ua (IV); popovaelp1642@gmail.com (EP)

for every 22 yr because the leading magnetic polarity of sunspots is shown to change every 11 yr (Hathaway, Wilson & Reichmann 2002; Hathaway 2015), (see also Livingston, Penn & Svalgaard 2012; Nagovitsyn, Pevtsov & Livingston 2012) and managed to reduce noise levels in the standardized sunspot numbers by accounting for smaller and more sporadic individual spots (see e.g. Hathaway 2013; Carrasco et al. 2018).

Svalgaard & Schatten (2016, 2017b) revisited the issue and brought up-to-date the Group Number series (Hoyt & Schatten 1998b). Svalgaard & Schatten (2017b) compared four reconstructions of the number of sunspot groups ('active regions') restored by different authors with different methods for the period since AD 1900 where the solar data are of sufficient quality. Despite severe criticism of the research by Svalgaard & Schatten (2016, 2017b) on the procedural grounds (e.g. Lockwood, Owens & Barnard 2016), this criticism was successfully dismounted (Svalgaard & Schatten 2017c). In fact, it was shown that all these reconstructions agree with each other within a few per cent, if using the data since 1900 when the underlying sunspot data are plentiful and of good quality (Cliver 2016).

There are also a few other indices of solar activity besides SSN, e.g. Sunspot Areas (SSA), radio flux F10.7, total solar irradiance TSI, radio intensity FI, etc. which show very good agreement with each other for the periods of time when they are available (Hathaway 2015). For example, Chatzistergos et al. (2017), using a daisy chain process with backbone (BB) observers, calibrated probability distribution functions (PDF) and concluded the solar activity to be rather moderate in 18th–19th centuries while increased in the 20th century. Willamo et al. (2017) using the singular spectrum analysis did a new reconstruction of sunspot numbers marking the centennial variability of solar activity and the modern grand maximum occurring in the second half of the 20th century.

Usoskin et al. (2021) applied a Monte Carlo method to find the lengths and strengths of cycles outside grand minima, which were agreeable with those derived from the direct sunspot observations after 1750. The authors reported that only grand solar minima (GSMs) and maxima of solar activity can be confidently detected while reported noticeable shifts of sunspot maxima in some individual solar cycles in 17th–18th centuries.

Recently, Zharkova, Shepherd & Zharkov (2012) and Zharkova et al. (2015) suggested to use an additional proxy of solar activity – eigenvectors of the SBMF obtained from the Wilcox Solar Observatory (WSO) low resolution synoptic magnetic maps. By applying the principal component analysis (PCA) to the synoptic magnetic data for cycles 21–23 (Zharkova et al. 2012) and recently for 21–24 (Zharkova & Shepherd 2022) the key eigenvalues and eigenvectors were identified representing magnetic waves of the solar surface.

The first pair of eigenvectors covered by the largest amount of the magnetic data by variance, or principal components (PCs), reflects the primary waves of solar magnetic dynamo produced by the dipole magnetic sources (Zharkova et al. 2015). The temporal features of the summary curve of these two PCs show a close resemblance to the sunspot index of solar activity (Zharkova et al. 2015; Zharkova & Shepherd 2022). This similarity occurs despite the eigenvectors, EV, and sunspot index (SSN) representing very different entities of solar activity: poloidal magnetic field (EV) and toroidal magnetic field (SSN). This similarity allowed the authors (Zharkova et al. 2015) to suggest the summary curve of the two PCs as a new, or additional, solar activity proxy.

The advantage of using the summary curve as solar activity proxy is the usage of real EVs of the poloidal magnetic field oscillations, derived from the magnetic field measurements and the fact that they are expressed by mathematical formulae as a function of time. This proxy introduces an extra-parameter, a leading polarity of SBMF (Zharkova et al. 2015), which is shown to be in antiphase with the magnetic polarity of leading sunspots (Zharkov, Gavryuseva & Zharkova 2008).

The summary curve, calculated backward 1200 and forward to 3200, reveals the very distinct variations of 11 yr cycle amplitudes in every 350–400 yr, or grand solar cycles (GSCs). These GSCs are separated by the GSMs when the 11 yr cycle amplitudes become very small, similar to those reported for Maunder, Wolf, Oort, and other GSMs. The summary curve has also shown the modern GSM to occur in the cycles 25–27, or in 2020–2053 (Zharkova et al. 2015; Zharkova 2020).

The timings of GSMs are defined by the interference (so-called beating, or summation of cosines, effect) of two magnetic dynamo waves with close but not equal frequencies defined by slightly different frequencies of the oscillations of two magnetic waves generated in different layers of solar interior (Zharkova et al. 2015). These different frequencies can be caused either by occurrence of two layers with slightly different velocities of meridional circulation in Zhao et al. (2013) and Zharkova et al. (2015), or by interference of the dynamo waves generated at the bottom of the Solar Convective Zone (SCZ) with natural oscillations of the solar interior.

It was also shown that these variations of the summary curve of SBMF are also linked to some volcanic events, which show some different patterns before and after 1860 when a strong geomagnetic jerk was reported (Newitt & Dawson 1984; Newitt et al. 2002). The summary curve of SBMF is shown to correlate very closely (correlation coefficient 0.84) with the frequencies of volcanic eruptions after 1860, while being weakly (0.23) correlated before 1860 (Vasilieva & Zharkova 2022; Vasilieva & Zharkova, in preparation). The volcanic eruption frequencies with high correlation coefficient are shown to be maximal during the maxima of solar cycles with the magnetic fields of southern polarity, which is expected during the next solar cycle 26 (2031–2042). The weak correlation, if the early sunspot data are included, is in line with the findings about large uncertainties with the sunspot index restoration in the 18th and mid-19th centuries (SS16; Svalgaard 2017).

The reduction of solar magnetic field and solar activity in cycles 25–27 was also predicted recently by the other researchers comparing the zonal harmonics of SBMF (Kitiashvili 2020; Obridko et al. 2021) derived from the same WSO synoptic maps of magnetic field used by Zharkova et al. (2015). In addition, the other reconstructions of sunspot cycles showed using singular spectral analysis (Courtillot, Lopes & Le Mouël 2021) prediction of lower sunspot numbers in cycle 25 or using Bayesian approach fitting the later cycles from 1850 towards the modern times the occurrence of the modern GSM in cycles 25–27 (Velasco Herrera, Soon & Legates 2021), similar to that predicted by Zharkova et al. (2015). Although, the later Bayesian fit of the whole series of sunspot cycles including those in 17th century (Velasco Herrera et al. 2022) reveals a good correspondence of the model cycles to the sunspot cycles while not matching the cycle durations or times of their maxima.

These findings raise significant interest to a comparison of the sunspot activity indices with the index derived from eigenvectors of SBMF (Zharkova et al. 2015). The overview of solar activity indices defined by sunspots and uncertainties in their definition are presented in Section 2, including recent restoration of the sunspot index with Bayesian method while a comparison of the summary curve of eigenvectors derived from the SBMF synoptic maps with the sunspot index described in Section 3 and the conclusions are drawn in Section 4.

2 SOLAR ACTIVITY INDICES: AVERAGED SUNSPOT NUMBERS

Most of our knowledge about sunspots in the 18th century relies on sunspot drawings by J.C. Staudach (digitised by Arlt 2008). The current averaged sunspot numbers are provided by SILSO World Data Center (2021) from 1730 until present.

2.1 Historical sunspot data: collection and problems

Observations of sunspots were carried out since 17th century in different countries without any systematic approach to generalize the observations loosing the interest towards the end of the century (see Fig. 1, top plot) believing that the appearances of sunspots were accidental. From the middle of the 18th century, the number of observations has increased by a number of observers (Wolf 1877; Dreyer 1903; Svalgaard 2017). Information about solar activity in the period 1749–1799 is based primarily on data from only two observers: Christian Horrebow and Johann Caspar Staudacher (Hoyt & Schatten 1998b) while the reconstructions of sunspot numbers during these years diverge significantly (Hathaway 2015; Karoff et al. 2019).

Then based on the records of daily observations between 1826 and 1843, Schwabe (1843) discovered a frequency of occurrence of sunspots with a cycle to be ∼10 yr. Later Rudolf Wolff redefined the duration of a solar cycle finding the maximum number of spots to be repeated every 11.1 yr (Wolf 1852). Wolf (1877) introduced a system of Wolf sunspot numbers (WSN), where the number of sunspots per day was determined by the main (preferred) observer. If the main observer was unable to count, then the definition from the secondary or tertiary observer with different weights was used. For each observer the individual observations are used to compute, first, monthly averages, then yearly averages from the averages of all months, if in this year at least one observation is carried out.

A primary observer was selected based on length of the observational series (as long as possible) and on the perceived 'quality' of sunspot observations, e.g. suitable telescope, regularity of observations, and a lack of detected problems. From 1849 to 1893, Wolf himself was the main observer, then the others were used: Alfred Wolfer (Zurich) from 1894 to 1926, William Otto Brunner (Zurich) 1926–1944, and Max Waldmeier (Arosa) 1945–1979. In the current times, the International Sunspot Number has been provided since 1981 by the Royal Observatory of Belgium with Sergio Cortesi (Locarno) as the main observer.

Wolf expanded the records 100 yr back, using Johann Kaspar Staudacher (Nuremberg) as the main observer from 1749 to 1787, Honore Flogerga (Vivier) from 1788 to 1825, and Samuel Heinrich Schwabe (Dessau) from 1826 to 1847. The scientists made very detailed sketches of the structure of sunspots, which are not lower quality in detail to even the best images taken with modern telescopes.

2.2 Recent restorations of the sunspot data

2.2.1 General comments

A significant step in improving the sunspot series was made in 1998 by Hoyt & Schatten (1998a, b; HS98 thereafter) who published a revised sunspot series with sunspot groups (GSN) from 1610. The GSN series of Hoyt & Schatten (1998b) is found to be more consistent and homogeneous with Schwabe's data throughout the entire studied period as found by Leussu et al. (2013), whereas the WSN records decreased by roughly 20 per cent around 1848 because of the change of the primary observer from Schwabe to Wolf. Although, the GSN reconstruction becomes very similar to WSN before the 1.25 correction factor was applied (Hoyt, Schatten & Nesme-Ribes 1994).

Clette et al. (2014) reported about a noticeable trend found and eliminated in the solar activity index derived from the observations of the Locarno Observatory, which was a reference observatory after 1980. Also, Clette et al. (2014) derived the three-peak shape (so-called Ψ-type distribution) of the original GSN by Hoyt & Schatten (1998a, b) for sunspot Cycle −1 with the peaks in 1736, 1739, and 1741. Later a modified single peak shape for this solar cycle was suggested by a number of authors (see, e.g. Usoskin et al. 2004; Vaquero 2007; Vaquero, Gallego & Trigo 2007; Vaquero & Gallego 2014) after more historical records of sunspot counts were discovered. Although, the derivation by Clette et al. (2014) indicated that the real shape of cycles in early years is not yet confirmed.

Then an almost 400 yr history of sunspot activity from 1610 to the 2000s was revised by joint efforts of researchers (Svalgaard & Schatten 2016, 2017a, b). Svalgaard & Schatten (2016; SS16 hereafter) has recounted the groups (and spots) for the present analysis and they use that recount as the base against which to normalize the counts by other observers. In order to bridge the gap with a poor overlap between the Schwabe and Staudach BBs and by examining the data for the decades surrounding the year 1800 when the change of the lead observer happened, SS16 concluded that the group counts reported by these observers during that interval can fall into two categories: 'low count' observers and 'high count' observers.

It was found (SS16) that overall, Wolf undercounted the number of groups by ≈25 per cent, while the counts of sunspots by these authors agree closely with Wolf's one. Although, the results by SS16 for cycle −10 do not agree with that by Hoyt & Schatten (1998b), whereas Lockwood, Owens & Barnard (2014) found that the shape −10 was similar to that of Hoyt & Schatten (1998b). The authors also concluded that solar activity in the 20th century was not much higher than that in the 18th century (SS16; Svalgaard 2017), whereas the uncertainties in sunspot restoration in the 18th and mid-19 centuries were much higher than after 1900.

Recent data revision of potential periods of sunspot maxima and cycle durations derived from the carbon ^{14}C isotopes in the trees is shown the shifts in 18th century of some maxima of sunspot numbers to the early years (Usoskin et al. 2021). This highlights the fact that sunspot indices in the first 15 cycles are based on unreliable data or the data with many wrong attributes not known then to the person building the sunspot index.

Since July 2015, the SILSO International Data Center (Sunspot Index and Long-term Solar Observations) at the Royal Observatory of Belgium maintains a new, revised series of relative sunspot numbers SSN (Version 2.0), which was considered to be fairly reliable since 1750 (Leussu et al. 2013; Clette et al. 2014; SS16). This solar activity data associated with averaged sunspot numbers SSN (V2) will be used here for a further comparison (see Fig. 1 bottom plot).

The main advantages of the corrected version SSN Version 2.0 are as follows:

(i) the usage as basis of observational series of Alfred Wolfer making them comparable with modern sunspot definitions;

(ii) the usage after 1947 of the weights introduced by Waldmeier (1961) in accordance with a size of the sunspots;

(iii) the elimination of a noticeable trend in the solar activity index derived from the observations of the Locarno Observatory, a reference observatory since 1980 (Clette et al. 2014).

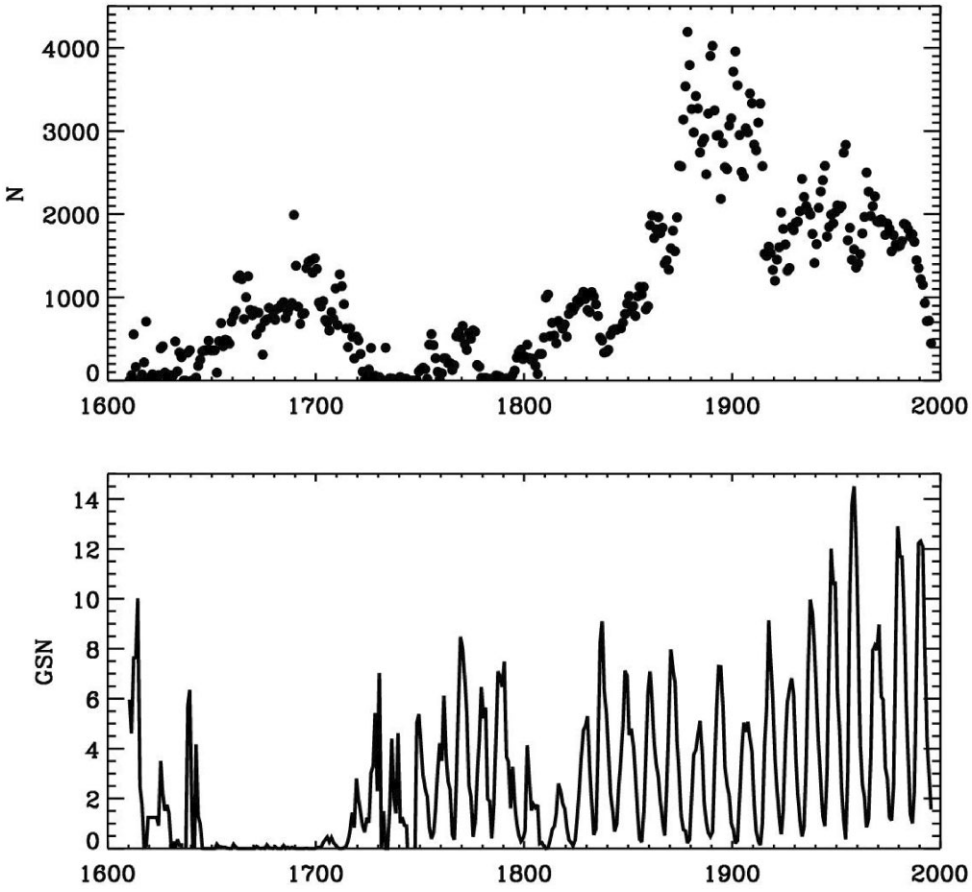

Figure 1. Top plot: The number N of observations per year used to reconstruct the averaged sunspot numbers. Bottom plot: The averaged sunspot numbers reconstructed from 1600 until the present time (SILSO World Data Center 2021).

The available observations of sunspots for given periods are summarized in Fig. 1, bottom plot (Vasiljeva & Pishkalo 2021). The maximum number of sunspots was observed in the 19th cycle (285.0) and the minimum number of sunspots was observed in the sixth cycle (81.2). The shortest and longest cycles were respectively the second and fourth cycles with the duration of 9.0 and 13.58 yr (Vasiljeva & Pishkalo 2021).

2.2.2 *Wavelet analysis of the averaged sunspot numbers SSN*

In order to detect the main periods in given series, we use a wavelet analysis with Morlet mother wavelet $\Psi(\eta)$ utilizing the main steps described in the summary of the Program in of Atmospheric and Oceanic Sciences, University of Colorado, of the usage of wavelets in Astrophysical applications (Torrence & Compo 1998). The Morlet wavelet analysis was applied to detect the frequencies (or periods) of averaged sunspot numbers as it is the most suitable mother wavelet to detect multiple periods in a temporal series (see section 3 in Torrence & Compo 1998). The results of Morlet wavelet analysis are plotted Fig. 2 with the original series of sunspot numbers presented in the top left plot, the wavelet spectrum in the bottom left plot, the colour bar of wavelet power shown in the top right plot and the global wavelet (solid black line) and Fourier (indigo line) spectra (see sections 5 and 4, respectively, in Torrence & Compo 1998) presented in the bottom right plot.

Since we use the finite-length temporal series, the errors occurring at the beginning and end of the wavelet power spectrum are controlled with the COI indicating the edge effects in the wavelet spectrum (see section 3g in Torrence & Compo 1998); COI is marked with the black dashed line in the wavelet spectrum in Fig. 2, bottom left plot. The periods detected by the wavelet analysis are verified by the global (smoothed) wavelet spectrum defined by formula (16) in section 5a of Torrence & Compo (1998), presented in Fig. 2, bottom right plot, by the solid black line. The black dashed line in the global wavelet spectrum shows the 95 per cent confidence interval of the wavelet spectrum as discussed below. The detected peaks in the wavelet spectrum, linked by convolution theorem to the Fourier transform [see formula (4) and Section 3h in Torrence & Compo (1998)], are also verified by the Fourier spectrum shown by the indigo line in the same Fig. 2, bottom right plot.

In order to evaluate the significance level of the detected wavelet results, we assume that the background spectrum of the wavelet as a red-noise spectrum with the increasing power when its frequency decreases. Since the Morlet wavelet is a series of bandpass filters of a time-series, we used Monte Carlo simulations to produce the red-noise local wavelet spectrum as described in section 3 of Torrence & Compo (1998). In this case, if the peak of a wavelet spectrum is significantly above this red-noise background spectrum, then this peak can be considered statistically significant with 95 per cent of confidence. The definition states (see section 4c in Torrence & Compo 1998) 'a significance at 5 per cent level is equivalent to the 95 per cent confidence level and implies a test against a given background level. At the same time, the definition of the 95 per cent confidence interval defines the range of confidence about the given value'. Then for a

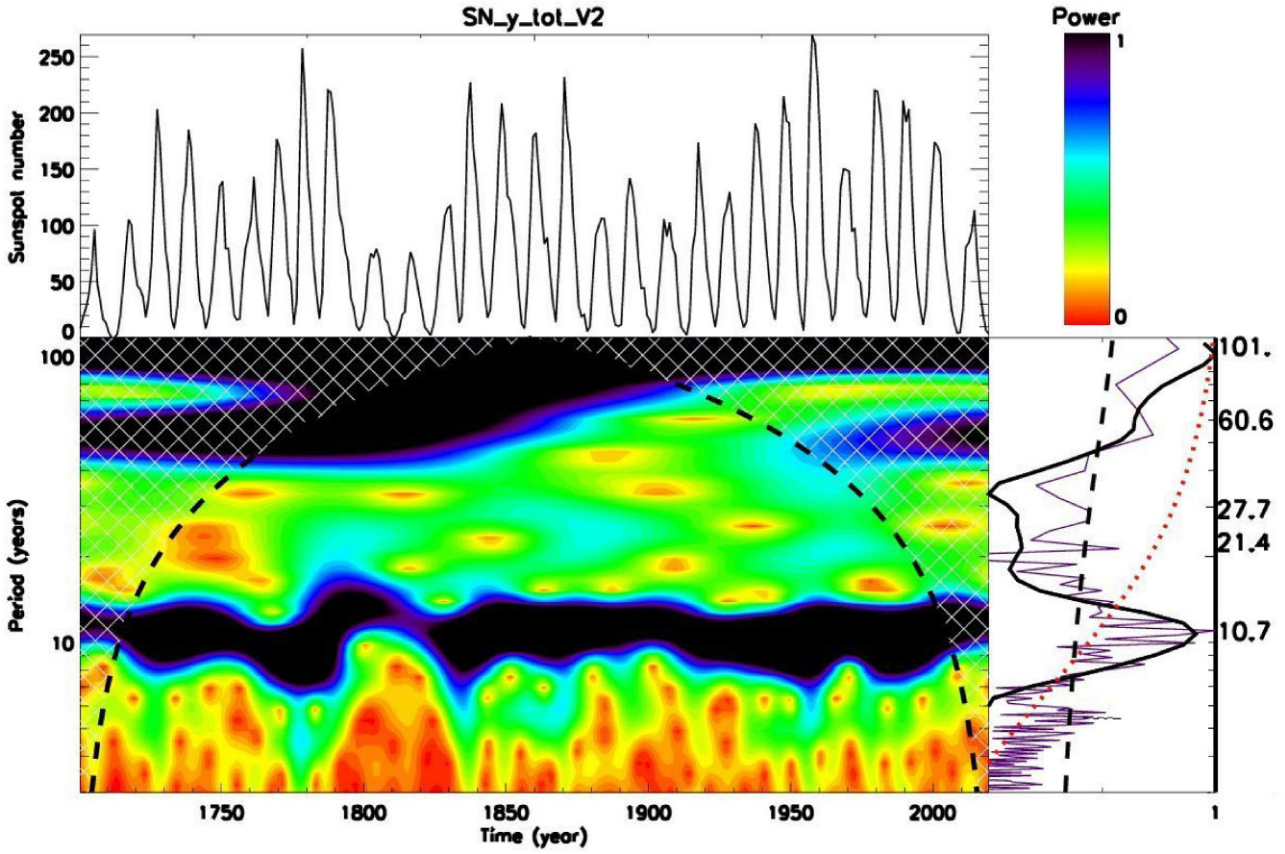

Figure 2. Left top plot: The averaged sunspot numbers SSN versus time in 1700–2020 including purely defined cycles. Left bottom plot: Wavelet spectrum with periods (*Y*-axis) derived from sunspot numbers with the black dashed line showing the cone of influence (COI) (see the text for details). Right top plot: The power bar for the wavelet spectrum. Right bottom plot: The global wavelet spectrum plotted by the solid black line, the black dashed line shows the 95 per cent confidence interval for the wavelet spectrum. Fourier spectrum is marked by the indigo line. The red-noise of the wavelet spectrum at the 95 per cent confidence level shown by the red dotted line. For details see the text in Section 2.2.2.

given background spectrum by using formula (18) in Torrence & Compo (1998) and defining the confidence for Ξ^2 to be 95 per cent it is possible to construct the contours of 95 per cent confidence level and then 95 per cent confidence interval.

This introduction explains the various curves obtained with wavelet analysis presented in Fig. 2. The 95 per cent confidence interval of the global wavelet spectrum is marked by the black dashed line in Fig. 2, right plot, the dashed red line denotes the red noise of the wavelet spectrum within the confidence interval of 95 per cent. Note that the power of the red noise grows with a reduction of frequency, e.g. with the growth of a period of oscillations. The peaks of the global wavelet spectra above the confidence level of 95 per cent (marked by the black dashed line) are considered to be significant.

The wavelet spectrum of temporal series of the averaged sunspot number reveals the powerful significant peak at 10.7 yr (corresponding to an 11 yr cycle) detected well above the required 95 per cent confidence level. There are also indications in the global wavelet spectrum of two larger periods: 60.6 and 101 yr. The first period of 60.6 yr appears as a bump well below the black dashed line (defining the 95 per cent confidence level) and much lower than the red dotted line defining the red noise at 95 per cent confidence interval. The second period of 101 yr associated with Gleissberg's centennial cycle is detected as the peak well above the black dashed line pointing to the 95 per cent confidence level while at the edge of the red noise at 95 per cent confidence interval. The Fourier spectrum shows peak at 100 yr, a wide-but-low bump in the Fourier spectrum for the period of 60 yr, some smaller peak at about 2.5–3 yr and a sharp but not high increase at the period of 21.4 yr that can be related to the biennial cycle and double 11 yr cycle. Their occurrences were suggested to be treated as stochastic noise (Cameron & Schüssler 2013, 2019), although these could be real peaks. Further investigation of this point is discussed in Section 3.1.3.

Hence, a wavelet spectrum of the sunspot numbers clearly detects a period of 10.7 yr while has some indication of larger periods of 60.6 and 101 yr. The absence in the wavelet spectra of a double period (21.4 yr) of the single period of 10.7 yr, signs of which are seen only in Fourier spectrum, is fully understood in terms that the sunspot numbers are scalar magnitudes, which do not have magnetic polarity indicated in their numbers, thus, they do not have the criteria to distinguish the periods of 21.4 yr associated with varying magnetic polarity of leading sunspots. Hence, for the scalar sunspot numbers only the 10.7 yr period is detectable. The two larger periods of 60.6 and 101 yr are detected below or at the edge of the 95 per cent confidence interval of the red noise. These periods appear to be less confidently detected because of a short length (320 yr) of the whole sunspot data set, so that they would require further investigation as suggested by Le Mouël, Lopes & Courtillot (2017) and Cameron & Schüssler (2019).

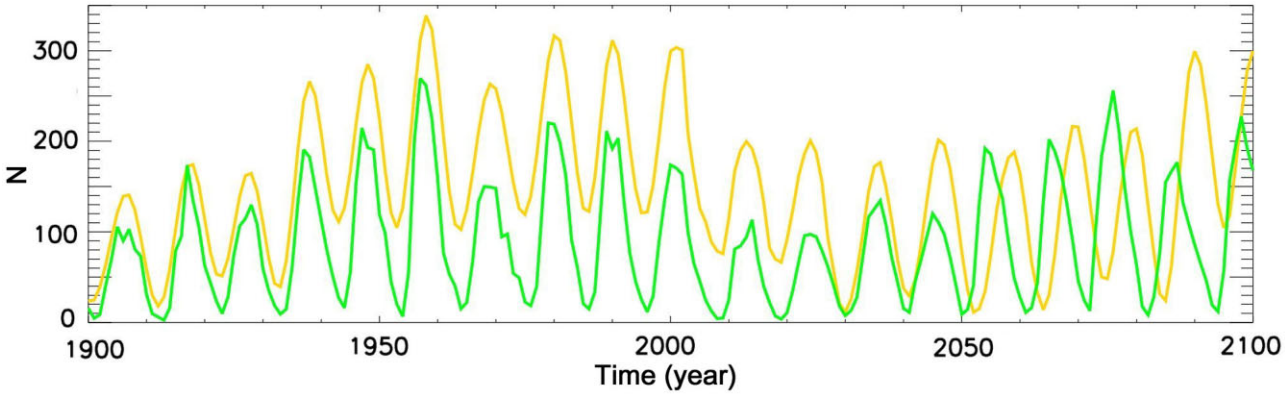

Figure 3. A comparison of the PMOD reconstruction with Bayesian approach (orange line) (VH21) with the sunspot reconstruction (green line) (VH22).

2.3 Discrepancies with fitting the averaged sunspot numbers

2.3.1 Bayesian fitting of sunspot numbers

There are two reconstructions VH21 and VH22 of the solar cycles represented by sunspots produced by the same group of authors (Velasco Herrera et al. 2021, 2022), which reveal slightly different temporal patterns. Velasco Herrera et al. (2021; VH21 hereafter) explored for restoration of averaged sunspot numbers from 1850 using the capacity of the Bayesian inference for Least-Squares Support-Vector Machines (LS-SVM) regression to forecast the expected number of sunspots for the future cycles until 2100. In the later paper (Velasco Herrera et al. 2022), the authors extended their model for a description of the whole set of solar activity indices defined by GSN series (Hoyt & Schatten 1998b) in cycles 1–25 and made the prediction to the cycle-10 (early 17th century). Their fitting really depends on, which part of the sunspot data the Bayesian approach was focused on, as shown in Fig. 3 by the green curve (VH21) and yellow curves (VH22).

If the Bayesian model was fitted to the cycles from 1850 until present (VH21), it restores the sunspot cycles correctly and shows the modern GSM to occur in cycles 25–27. However, If the Bayesian model was fitted by the whole series of sunspot cycles (VH22), then the solar activity cycles 25–27 are not significantly reduced and the cycles are shifted forwards in time after 2050 as shown in Fig. 3 by comparing the green (VH21) and yellow curves (VH22). Although, the orange curve VH22 shows a good fitting of Maunder minimum and most of the cycles between 1800 and 1950 while struggling to fit some very early cycles when there were little observations and the later solar cycles in 21st century.

Hence, in addition to the general problems with building the averaged sunspot numbers listed in the previous section, there are remaining problems affecting the sunspot index if fitted by the Bayesian methods. Bayesian fitting centred either to 18th–19th century data or towards 20th–21st century data produced the arrays, which do not exactly coincide in the intermediate points. This correlates with the recent data revision of sunspot maxima and cycle durations with carbon 14 isotope data showing in the years in 18th century some shifts of the maxima dates to the dates where originally were minima. These discrepancies could be caused by the problems with the sunspot identification appeared from the early data as described below.

2.3.2 Estimated uncertainties of sunspot fitting

The known problems with the establishing sunspots times and locations as well as deriving the solar activity index in early years:

(i) Unexperienced drawings by some observers in early years.
(ii) Poor observations by some observers leafing to the difficulties to build a BB.
(iii) It is unknown if the number of sunspots in groups changes over time.
(iv) Accounting for years with less than 20 observation days per year that brings large errors.
(v) The impossibility of determining the weighting factor for the periods with a single observer.
(vi) There were different calendars (Julian versus Gregorian) used until mid- or late 18th century in different countries where the dates placed on drawings did not indicate which calendar had been used.
(vii) In a few key countries there were different starts of a New Year (April in Britain, September in Russia, etc.) used meaning that unless recorded, the year on the sunspot drawings also would not correspondent to the accepted calendar year.

Although the items 1–5 were actively discussed numerous times in the most papers cited above exploring various solar activity indices, the items 6 and 7 were avoided from this attention while they can contribute with the major errors in defining solar cycles maxima and durations.

The problems with early cycles in 18th century are likely caused by the absence or scarceness of the observations (see Fig. 1), which cannot be repaired unless more historical data are found. Furthermore, in the 18th century many countries were moving from Julian calendar to Gregorian one in very different times (see the table https://en.wikipedia.org/wiki/List_of_adoption_dates_of_the_Gregorian_calendar_by_country). These calendar moves happened in different years in different countries and not always was the calendar indicated in the drawings used for the sunspot index definition. Therefore, reliability of the sunspot data in these years is rather questionable.

To complicate the matters the different countries had different starts of their years. In Britain a New Year Day was March 25th until it was changed to the January 1st in 1751, the Gregorian Calendar was adopted in 1752 with 11 d being 'lost' in September of that year. Hence 1750 was only 40 weeks in duration and 1752 just over 50

weeks. This meant that, e.g. the drawings made in January–March 1750 by the old calendar without marking the calendar used and a year start, actually belonged to the next year 1751 and so on. The similar discrepancies could occur with the drawing carried in the country where the year start was September or the other months. These objective problems led to some very strange solar cycles derived for the 18th century, when the cycle lengths were either 7 or 8 yr while other cycles lasted for 15 yr.

These discrepancies raise more questions to the quality of solar activity index defined by the sunspot data used currently by many restorations as the sunspot cycles in 18th–19th centuries. None the less, a use of this familiar sunspot indices, either Wolf numbers WSN or sunspot numbers SSN, are well accepted by the solar-terrestrial community, despite any discrepancies and difficulties they experience with the replication of these solar activity (SA) indices. We fully appreciate tremendous efforts of the solar community to this topic, which helped researchers to understand the nature and need of solar activity indices and to improve their accuracy in the modern days as far as it is feasible with a sunspot proxy.

However, for the sake of diversity, it is worth to look at some other possibilities to define solar activity, like Bayesian models shown here (VH21 and VH22) or to use PCA index recently suggested (Zharkova et al. 2015; Zharkova & Shepherd 2022) for a comparison with the accepted index of solar activity with the averaged sunspot numbers.

3 SOLAR ACTIVITY INDEX FROM THE EIGENVECTORS OF SBMF

3.1 Pair of eigenvectors, or principal components

3.1.1 Two PCs and their summary curve

The dynamo mechanism, which governs solar activity, operates with poloidal and toroidal magnetic fields (Parker 1955), with the first one being the SBMF, and the second one being the field of magnetic loops in active regions, which are embedded into the solar surface, whose roots are seen as sunspots. The interaction between these two magnetic fields defines the variations of solar activity seen through the appearance or disappearance of sunspots and active regions.

The two PCs, or eigenvectors, of the SBMF are calculated by applying the PCA to the Wilcox Solar Observatory low resolution full disk synoptic magnetic maps for cycles 21–23 (1976.4–2006.0) (Zharkova et al. 2012) and cycles 21–24 (1976.4–2021.5) (Zharkova & Shepherd 2022). The authors identified numerous eigenvalues and eigenvectors of own magnetic waves of the Sun seen on the solar surface, which came in pairs. The four significant pairs covering the majority [$>$ 95 per cent of the data by variance (Zharkova et al. 2012; Zharkova & Shepherd 2022)].

The first pair, or two PCs, reflects the primary waves of the solar magnetic dynamo produced by dipole magnetic sources (Zharkova et al. 2015). These two waves are found traveling slightly off-phase from one hemisphere to another and their interaction define the solar activity in each hemisphere and as a whole (Zharkova et al. 2012). Shepherd, Zharkov & Zharkova (2014) and Zharkova et al. (2015) used the symbolic regression analysis (Schmidt & Lipson 2009) of these two magnetic waves and obtained the analytical expressions for the magnetic (dynamo) waves incorporated into the ensemble of waves present in the SBMF attributed to the poloidal field of the Sun (Popova, Zharkova & Zharkov 2013). These mathematical equations were used to make predictions in time by 1000 yr both forward and backward, from the current epoch and to use them for a comparison with the magnetic waves supposedly produced by the solar dynamo acting in two layers with slightly different meridional circulation velocities (Zharkova et al. 2015).

The SBMF is shown to be in antiphase with the leading polarity of magnetic field in sunspots (Stix 1976; Zharkov et al. 2008), thus, defining the locations and timing of sunspot appearances on the solar surface and their migration towards the solar equator or poles (Zharkov et al. 2008). Therefore, in order to bring the detected trends in the SBMF closer to the currently used index of solar activity, averaged sunspot numbers, the summary component of the two PCs was calculated. The modulus summary curve (MSC) was found to correlate closely with averaged sunspot numbers (Shepherd et al. 2014; Zharkova et al. 2015; Zharkova & Shepherd 2022) that suggested the summary curve of these two PCs can be used as a new proxy of solar activity, in addition to the current solar activity index of the averaged sunspot numbers.

Using the derived formulae, the summary curve was calculated backward to 1200 and forward to 3200 (Zharkova et al. 2015) as shown in Fig. 4, top plot revealing very distinct variations of the cycle amplitudes in every 350–400 yr, or grand solar cycles (Zharkova et al. 2018b). These grand solar cycles are separated by GSMs, when the amplitudes of 11 yr cycles become very small, similar to those reported in Maunder, Wolf and Oort and other GSMs (Zharkova et al. 2018a, b).

The current grand solar cycle (GSC) shown in Fig. 4, bottom plot started during Maunder Minimum and is predicted to continue until the modern GSM (2020–2053) as pointed by Zharkova et al. (2015). The recent research of the same SBMF data of WSO (Kitiashvili 2020; Obridko et al. 2021) also found that the SBMF is reducing towards cycles 25–27, similar to the predictions by Zharkova et al. (2015) for the summary curve of two largest eigenvectors of SBMF

The summary curve is shown to represent a clear physical process – dynamo waves of solar poloidal field generated by the dipole magnetic sources in two layers of solar interior (Zharkova et al. 2015). The timings of the GSMs were interpreted as the interference of two magnetic dynamo waves generated in different layers with close but not equal frequencies that are defined by slightly (by about 1 m s^{-1}) different velocities of the meridional circulation in two layers where these waves were generated (so-called beating effect; Zharkova et al. 2015). The calculation of the summary curve forward in time until 3200 has shown the further three grand solar cycles separated by GSMs with the first GSM to occur in cycles 25–27, or in 2020–2053 and other one in 2375–2415 (Zharkova et al. 2015; Zharkova 2020).

3.1.2 Modulus summary curve and the sunspot index

The modulus of the summary curve (MSC) of these two PCs ignores the sign of magnetic field (positive for northern polarity and negative for southern one) and reflects the curve to the positive numbers only. This makes MSC similar to sunspots and allows to compare for the same times with averaged sunspot numbers. This comparison shows a remarkable resemblance of MSC to the sunspot index of solar activity for cycles 21–23 (Shepherd et al. 2014; Zharkova et al. 2015), and recently, for cycles 21–24 (Zharkova & Shepherd 2022). Embracing the similarity between MSC and averaged sunspot numbers, the MSC can be normalized for each cycle by the averaged sunspot numbers indicated by the left *Y*-axis in fig. 9 of Zharkova & Shepherd (2022). The modulus curve, in general, follows the averaged sunspot numbers for all the the cycles revealing a significant reduction of solar activity from cycle 21

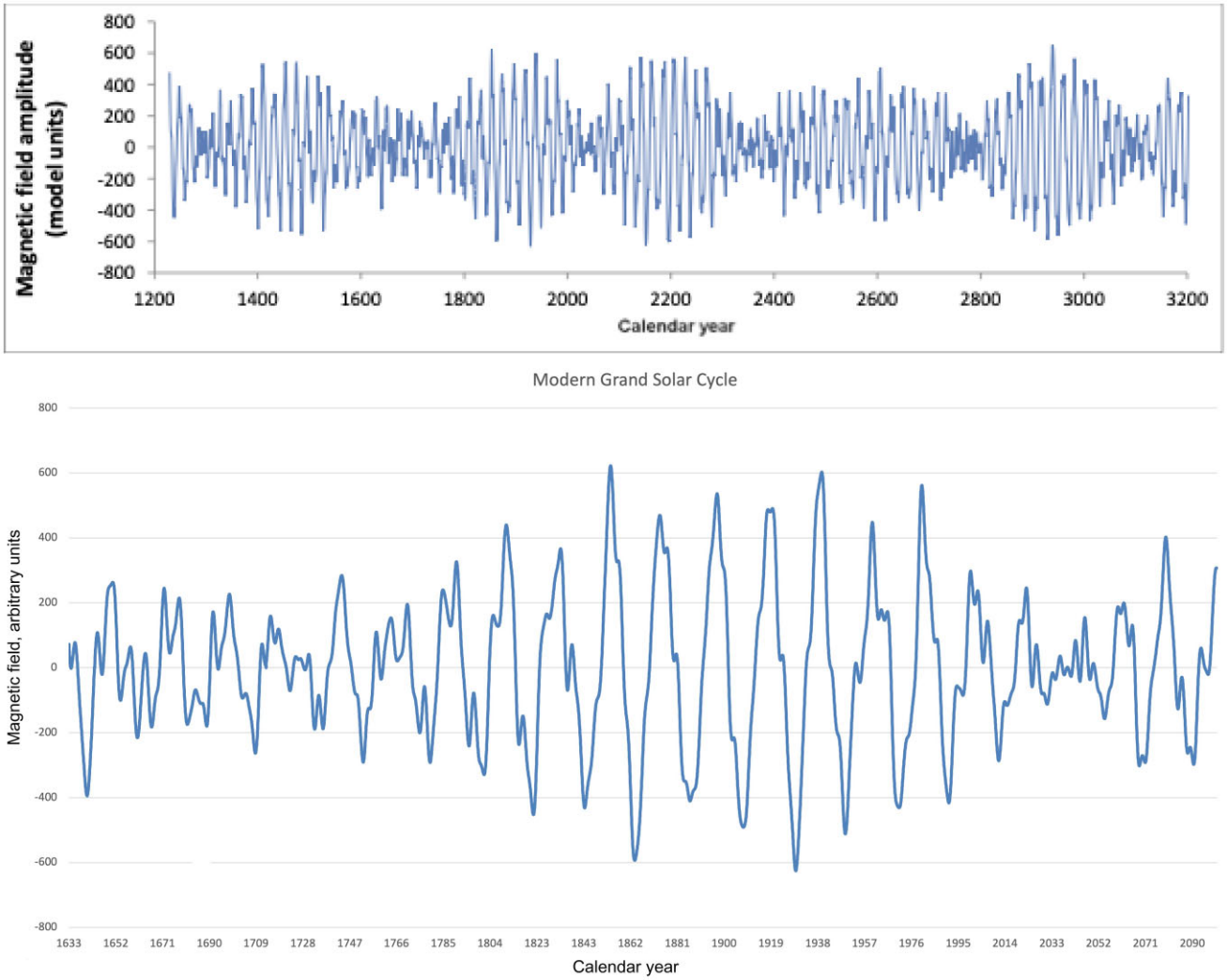

Figure 4. Top plot: The summary curve of two PCs (in arbitrary units) versus time calculated for 2000 yr (1200–3200) (Zharkova et al. 2015). Bottom plot: The summary curve (in arbitrary units) versus time from 1600 till 2100 yr taken from the top plot representing the current grand solar cycle including Maunder minimum (1645–1710) before it and modern GSM (2020–2053) after.

(maximum about 300 sunspots), through cycle 22 (230), 23 (165) to cycle 24 (108) (Zharkova & Shepherd 2022) that fits reasonably to the maximum numbers reported for cycles 21–24 (SILSO World Data Center 2021): 21–233, 22–213, 23–180, and 24–116.

These two curves, MSC and SSN, represent, in fact, different magnetic components of solar dynamo waves: poloidal for the MSC and toroidal for averaged sunspot numbers. The reasonable similarity of these two curves allowed authors (Zharkova et al. 2015) to suggest this summary curve of PCs, or eigenvectors of SBMF, as a new solar activity proxy. The advantage of using the solar index from the summary curve instead of the averaged sunspot numbers is a presence of extra-parameter, a leading polarity of the SBMF, and the ability to do long-term prediction of this index.

Therefore, the MSC proves that the eigenvectors of SBMF can be considered as complementary solar activity index, in addition to the existing one of the averaged sunspot numbers.This new index adds the additional parameter to this proxy – a dominant polarity of the SBMF for each cycle, which has the polarity opposite to the leading polarity of sunspots (Stix 1976; Zharkov et al. 2008).

3.1.3 Wavelet analysis of the MSC

Using the same methodology of the wavelet analysis described in details in Section 2.2.2, let us apply the wavelet transform to the MSC for 1000 yr (1200–2200) taken from our paper (Zharkova et al. 2015) and plot the results in Fig. 5. Here, is a brief summary of the presented results. The original MSC is plotted in Fig. 5, top left plot, the obtained wavelet spectrum – in the bottom left plot, the colour bar of the wavelet power is shown in the top right plot. The global wavelet spectrum (solid black line) and Fourier spectrum (Indigo line) are presented in Fig. 5, bottom right plot.

The black dashed line in the wavelet spectrum (bottom left plot) marks the COI defining parts of the spectrum where the boarder effects of a wavelet analysis become essential and, thus, excluded from the further investigation. The black dashed line in the global wavelet spectrum (bottom right plot) defines the 95 per cent confidence interval of the detected periods. The 95 per cent confidence level of the global wavelet spectrum is marked in Fig. 5, the right bottom image, by the dashed red lines denoting the red-noise of the wavelet spectrum calculated with Monte Carlo approach. Note that the power of the red noise grows with a reduction of frequency, e.g.

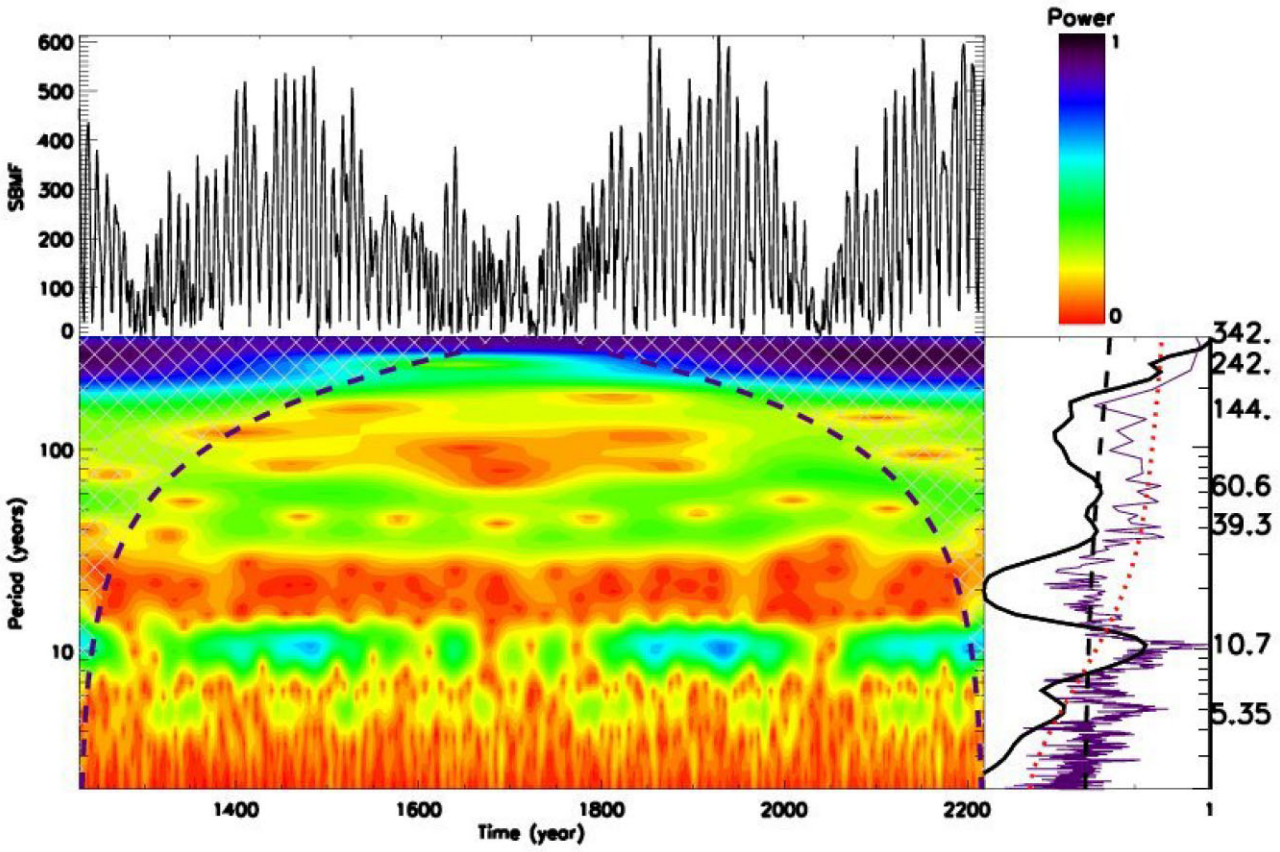

Figure 5. Left top plot: The MSC of SBMF in 1200–2200 (a courtesy of Zharkova et al. 2015). Left bottom plot: Wavelet spectrum derived from the MSC with the black dashed line showing the COI (see the text for details). Right top plot: The power bar for the wavelet spectrum shown in the bottom left plot. Right bottom plot: The global wavelet spectrum plotted by the solid black line, the black dashed line shows the 95 per cent confidence interval for the global wavelet spectrum. Fourier spectrum is marked by the indigo line. The red-noise of the wavelet spectrum at the 95 per cent confidence level is shown by the red dotted line (see the Section 3.1.3 for details).

with the growth of a period of oscillations. The peaks of the global wavelet spectra above the red noise at the confidence level of 95 per cent (red dotted line) are considered to be significant.

It can be seen that the wavelet spectrum of the MSC reveals the significant well-distinguished peak at 10.7 yr and another strong peak at the 342 yr, both appearing well within the 95 per cent confidence interval of the global wavelet spectrum (black dashed line) and above the 95 per cent confidence level of the red noise. The two similar significant periods of 10.7 and 342 yr appear also in Fourier spectrum. The first period of 10.7 yr has the same duration as the one found for the sunspot cycles reported in Section 2.2.2 for the averaged sunspot numbers. This is a good confirmation that the MSC oscillations occur with the same period as those of sunspot numbers, as one would expect from the action of dynamo mechanism in poloidal and toroidal magnetic fields generating these waves.

There are also some additional periods: a small hump in the global wavelet spectrum at the period of 242 yr at the edge of 95 per cent confidence level for red noise, two insignificant maxima in the global wavelet spectrum at the edge of 95 per cent confidence level for the global wavelet spectrum (black dotted line), and Fourier peaks at 60.6, 39 yr and 5.35 or lesser years. The periods besides 60.6 yr are not seen in sunspot numbers, which duration is limited by 320 yr. These additional periods can be real or they can be a statistical noise produced by the dynamo wave interference (Cameron & Schüssler 2013, 2019) that requires further investigation for each case separately.

For example, this wavelet spectrum of the MSC of the two PCs, or eigenvectors, reveals the absence of a period of 101 yr in the wavelet of MSC, while it was seen in the wavelet spectrum of the averaged sunspot number in Fig. 2. This absence of the centennial period in the MSC can be understood from the fact that the two PCs, or magnetic waves with largest eigenvectors, are shown produced by dipole magnetic field (Zharkova et al. 2015), which is mainly responsible for the basic solar activity cycle of about 11 yr. In order to obtain oscillations of centennial (Gleissberg) cycle of 80–101 yr, we need to add the magnetic waves generated by quadruple magnetic sources (Popova et al. 2018; Zharkova & Shepherd 2022), or the next pair of eigenvectors, which are not included yet into the summary curve presented in Fig. 4.

There is also a larger period of 342 yr detected with the wavelet analysis with the sufficient confidence well above the red noise and 95 per cent confidence interval in the global wavelet spectrum as shown in Fig. 5, bottom right plot. This larger period corresponds to a period of the grand solar cycle recorded during the selected 1000 yr (1200–2200) of the MSC that has need reported earlier from the eigenvectors of the SBMF (Zharkova et al. 2015). During this 1000 yr duration presented in this wavelet plot there were only

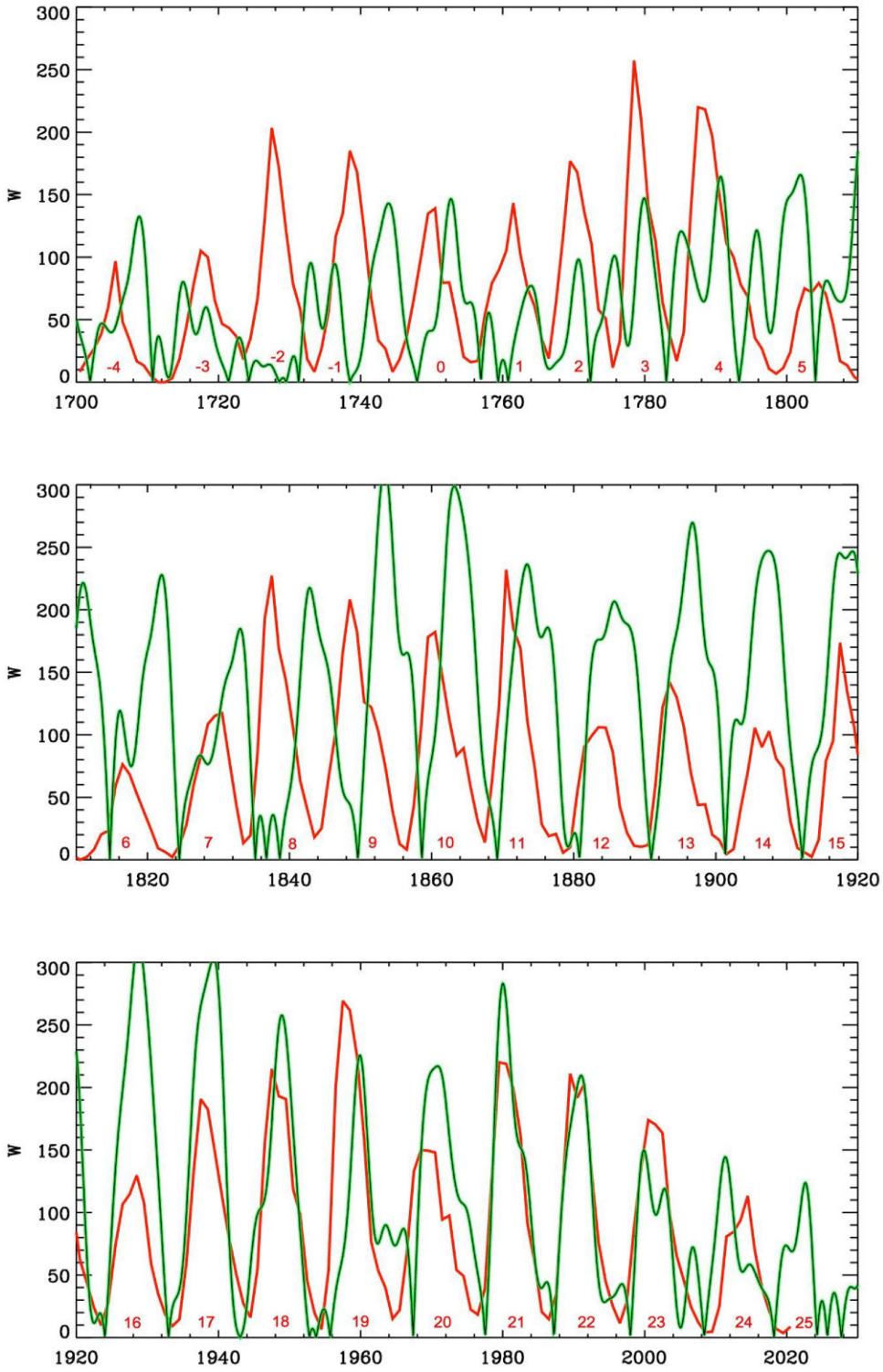

Figure 6. Comparison of the MSC (green line) (Zharkova et al. 2015) with the averaged sunspot numbers W (SSN) (red line) (SILSO World Data Center 2021). Numbers indicate the cycle numbers in SSN.

three grand solar cycles and three GSMs: Wolf minimum, Maunder minimum, and modern GSM (2020–2053). Hence, we can conclude that the wavelet analysis detected the real period of 342 yr of the grand solar cycles for the oscillation of amplitudes of 10.7 yr MSC cycles, similar to the sunspot cycles.

3.2 Comparing the MSC and averaged sunspot numbers

3.2.1 Direct comparison of the MSC and SSN curves

Here in Fig. 6, we present a comparison of the MSC (green line) (Zharkova et al. 2015) with the averaged sunspot numbers (red

line), from *https://wwwbis.sidc.be/silso/* (SILSO World Data Center 2021).

Based on some similarity of the modulus summary MSC and sunspot SSN curves in cycles 21–24 one can conclude that the solar activity in these cycles is systematically decreasing with a cycle number (Zharkova et al. 2015; Zharkova & Shepherd 2022) because of the shift in phase of the two magnetic waves in these PCs, shown in the summary curves in figs 2 and 3 in Zharkova et al. (2015) and in Fig. 4 here, which for the MSC is shown in Fig. 5 (top left plot). The phase difference between the two waves is increasing in time for cycles 25–27, approaching nearly the antiphase status in cycle 26 (see fig. 2 in Zharkova et al. (2015) and Figs 4 (top plot) and 5 (upper left plot).

This magnetic wave separation into the opposite phases will definitely lead to a reduction of the magnetic wave amplitudes in 11 yr cycles, e.g. the reduction of a magnetic flux of the SBMF and the significant reduction of magnetic loops on the surface, whose roots appear as sunspots. This process led to the reduction or even absence of noticeable magnetic activity on the solar surface occurred in the 17th century during the Maunder Minimum (MM; Spörer 1889; Eddy 1976; Ribes & Nesme-Ribes 1993), prior the current grand cycle. The similar process is also expected to be observed in cycles 25–27 (Zharkova et al. 2015) forming the modern GSM.

Hence, after the previous GSM during MM in the following 350 yr of the current grand solar cycle (GSC), considered here and shown in Fig. 4, bottom plot one can observe is a rather reasonable agreement between the MSC and SSN as in the average duration (10.7 yr) and the ratios of maximum amplitudes for cycles 12–24 as shown in the bottom and middle rows of the plots in Fig. 6. Although, the maximum amplitudes for cycles of the MSC curve systematically exceeding the SSN maximum magnitudes from cycle 12 to cycle 17 that is similar to the reconstructions reported by Solanki et al. (2004); Chatzistergos et al. (2017). While for earlier cycles from −4 to 5 the MSC maximal amplitudes are systematically lower than the averaged sunspot numbers.

We derive from the comparison of the MSC and SSN curves that the major discrepancies occur in the periods of 1730–1780 in the 18th century and in the period of 1830–1870 in the 19th century. In the 18th century some cycles in SSN had durations of 7 or 8 yr while others lasted for 15 yr while the MSC curve shows the appearance of an additional cycle between cycles 5 and cycle 6 (which in SSN was of 15 yr duration), a shifted duration for cycle 5, close durations between the MSC and SSN curves for cycles 1 and 4 with triple maxima in cycle 1. Also, there are MSC cycles slightly shifted forward compared to SSN in cycles −2 to 0 and close resemblance of MSC with SSN for cycles −3 to −4 occurring after the end of Maunder minimum.

More complicated relations with the MSC, or eigenvectors, defined from the SBMF appear for three cycles 8–10, cycles −2 to 1 and for cycles 4–6 and possibly 7. Cycles −2 and −3 in the MSC curve have shown three-peak shapes, similar to those reported by Clette et al. (2014) from the reconstruction by Hoyt & Schatten (1998b). Definitely, cycles 3–5 in the MSC curve, with a duration about 11 yr each, have two maxima shapes. These were followed by cycles 6 and 7 which have reduced first maxima and much larger the second ones while from cycles 8 onwards in the MSC curve is returning to cycles with single maximum shapes.

In the MSC, cycles 8–11 (Fig. 6, middle plot) are shifted forward from the SSN curve, slightly for cycle 11, more for cycle 10 and by a half of a cycle length for cycles 9 and 8, so that the maxima in cycle 8 and 9 in MSC occur during the minima in SSN. These are followed by correct durations for cycles 7 and 6. The duration of cycles 7 and 8 in the MSC curve resembles the duration of those for the sunspot curve, although the MSC cycles are slightly shifted forward in time compared with SSN. In cycles 8–10 the minima and maxima in sunspot index were overlapped the with the maxima and minima of the MSC cycles.

Then from cycle 11 the MSC curve shifts ahead the sunspot cycle by a year or by year and half and then follows the cycle durations of sunspot cycles being though higher in amplitudes. Note that the averaged duration of all cycles in the MSC curve is the same 10.7 yr like in the sunspot curve SSN as the wavelet and Fourier analysis confirmed in Sections 2.2.2 and 3.1.3.

3.2.2 Comparing different restorations of the sunspot indices before 1900

The plots for a few reconstructions of solar activity, or sunspot index, are shown in Fig. 7, demonstrating the locations of cycles and maximal magnitudes of sunspot activity according to different authors. A comparison of the solar activity cycles and newly found maxima of solar activity derived from the updated data of sunspots by different authors are shown in Fig. 7. The legend beneath the image and coloured arrows presents the maxima in restorations obtained by different authors: red arrows by Beer, Tobias & Weiss (1998), grey arrows by Maunder (1922), green arrows by Waldmeier (1961), orange arrows by Schove (1983), blue arrows by Velasco Herrera et al. (2022), and mustard arrows by Usoskin et al. (2021).

It can be seen that for some restorations of the sunspot index the discrepancy in the times of maxima of sunspot numbers between the different data including our curve MSC reached 5–6 yr (see also discussion in Kane 2008; Velasco Herrera et al. 2022). Some sunspot cycles considered to last only 7 or 8 yr while the others had a duration of 15 yr while the MSC curve shows more coherent cycle durations close to the averaged time of 10.7 yr with two, or sometimes three, maxima. The MSC maxima in the 18th–19th centuries are shown to be closer to those derived by Beer et al. (1998) or Velasco Herrera et al. (2022).

Furthermore, there was a very interesting development made in the recent data revision associated with the new sunspot activity restoration derived from the abundances of the isotope ^{14}C in the trees (Usoskin et al. 2021). The authors reported the shifts of the maximal magnitudes of sunspot numbers in the 18th century to the years where originally there were minima of sunspots (see Fig. 7). These shifts of the SSN maxima make them close to the maxima of the MSC reported by us from PCA (Zharkova et al. 2015) for this period for cycles from −2 to 0, and for cycles 8–11 as shown in Fig. 6, top and middle plots.

3.2.3 Statistical analysis of the MSC and SSN curves with SPSS

The rigorous statistical analysis was carried out of the correlation between the MSC and SSN curves using the SPSS package, v28 (see Fig. 8) presenting the scatter plots of Spearman correlation for different periods of observations of the averaged sunspot numbers from 1750 until present times associated with different accuracy of restoration as discussed in Section 2.3. In each scatter plot we plot the best correlation curve found with the linear fit (magenta line), show the two lines showing the 95 per cent confidence interval. For all the cases the correlation is significant at the 0.01 level.

First of all, the correlation coefficient between SSN and MSC is strongly dependent on the data accuracy. In the early years of observations from 1750 until 1900 when the problems with a number

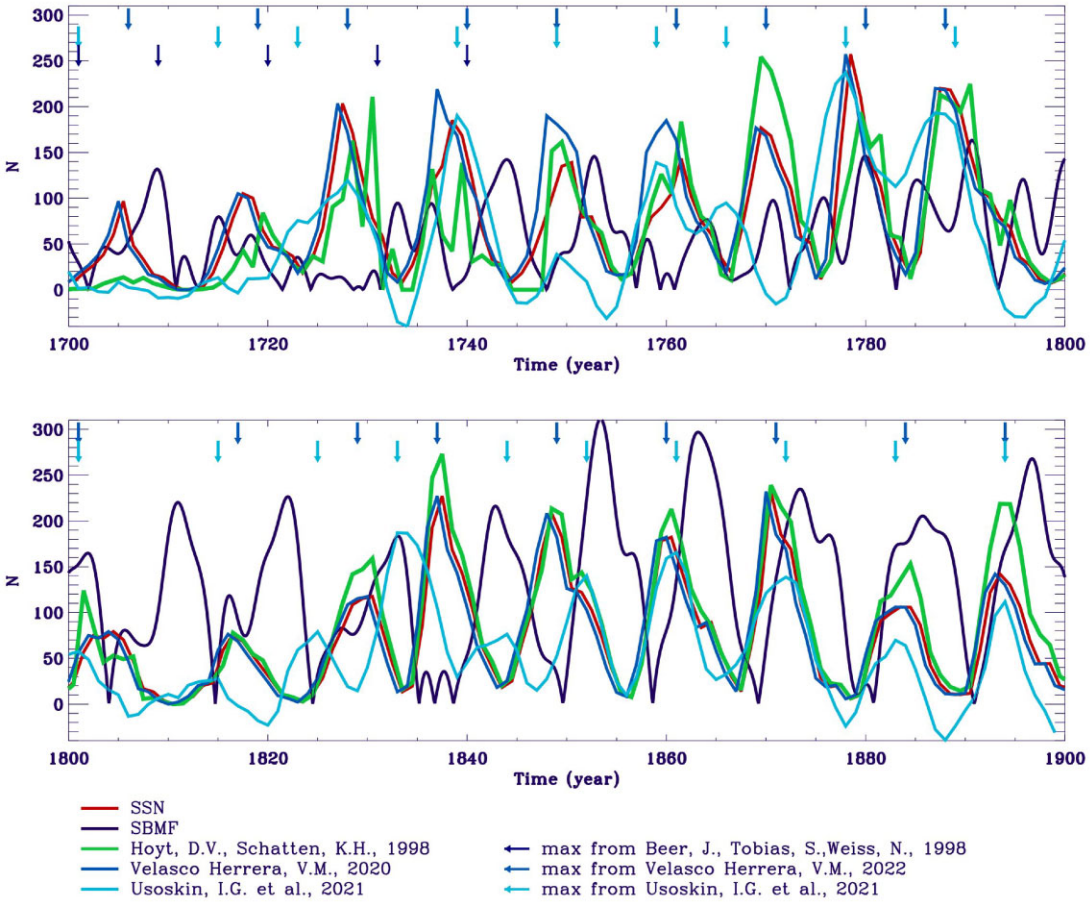

Figure 7. A comparison of the restoration of sunspot numbers *N* in 1700–1900 versus time done by different authors derived from sunspots with the MSC. The colour arrows on the top indicate the maxima derived by the relevant restoration from radioisotopes or Bayesian approach (see the legend beneath the plot).

of observations were present (SS16; Svalgaard 2017) like with the identification of the key observers or problems with various calendar dating issues or potential effects of geomagnetic jerk (Newitt & Dawson 1984; Newitt et al. 2002).

As result, if the whole early data are included, the correlation coefficient between SSN and MSC data is rather low (0.25). Then, if the sunspot and MSC data started from 1860, the correlation becomes more than twice higher (0.56) and, if the SSN and MSC data considered from 1900 when all the SSN restorations agree, it approaches the coefficient of 0.67. This is an indication that, similar to the SSN index, the summary curve of the two largest eigenvectors of SBMF covering 39 per cent of the magnetic data by variance, or 67 per cent by standard deviation, can be an additional proxy of solar activity that is discussed in Section 3.3.2.

Secondly, in order to demonstrate these correlations, the scatter plots are presented in Fig. 8 for each data set starting in 1750, 1860, and 1900 until the present times. We fit the linear and quadratic curves to the scatter plots to find a better data fitting, showing that quadratic approach gives a slightly better fit, following Ξ^2 values. It is evident that the data scatter for the whole SSN data set (Fig. 8, top plot) is pretty large following the problems with the observations in the 18th century shown in Fig. 1, bottom plot. The sunspot data uncertainties at that time are likely to reduce the correlation between the SSN and MSC curves to 0.25.

If the data are taken 110 yr after 1750, from 1860 till present time. (Fig. 8, middle plot), the data scattering becomes much smaller and the correlation coefficient is increased from 0.25 to 0.56. If one takes the most clean sunspot data after 1900 (Fig. 8, bottom plot) when the most sunspot restorations agree one with another, the correlation coefficient increases to 0.67 that is pretty reasonable for the entities produced by the different magnetic fields: poloidal for MSC and toroidal for SSN.

3.2.4 Forced fitting of the MSC to the SSN cycles

Let us make an attempt to fit as close as possible the parameters of observed averaged sunspot numbers SSN (SILSO World Data Center 2021). the parameters of the eigenvectors used in the MSC. The fitting was carried out using Hamiltonian regression approach by optimize a few key parameters to the MSC curve to fit thee SSN curve, like cycle periods, time of minima between cycles and maximal amplitudes, or cycle powers, varying in time. The fitting of the updated MSC to the existing SSN is shown in Fig. 9 for 11 yr cycles from 1750 until present.

This fitting is found to have essential limitations depending on the part, which we want to fit to the MSC from the sunspot index. This problem is similar to the problems found in Bayesian approach reported by VH21 and VH22 shown in Fig. 3. Namely, if we attempt to fit the MSC curve to the averaged sunspot numbers SSN for all the cycles of SSN including those from 1750 to 1860, the MSC curve fits rather closely the cycle durations and

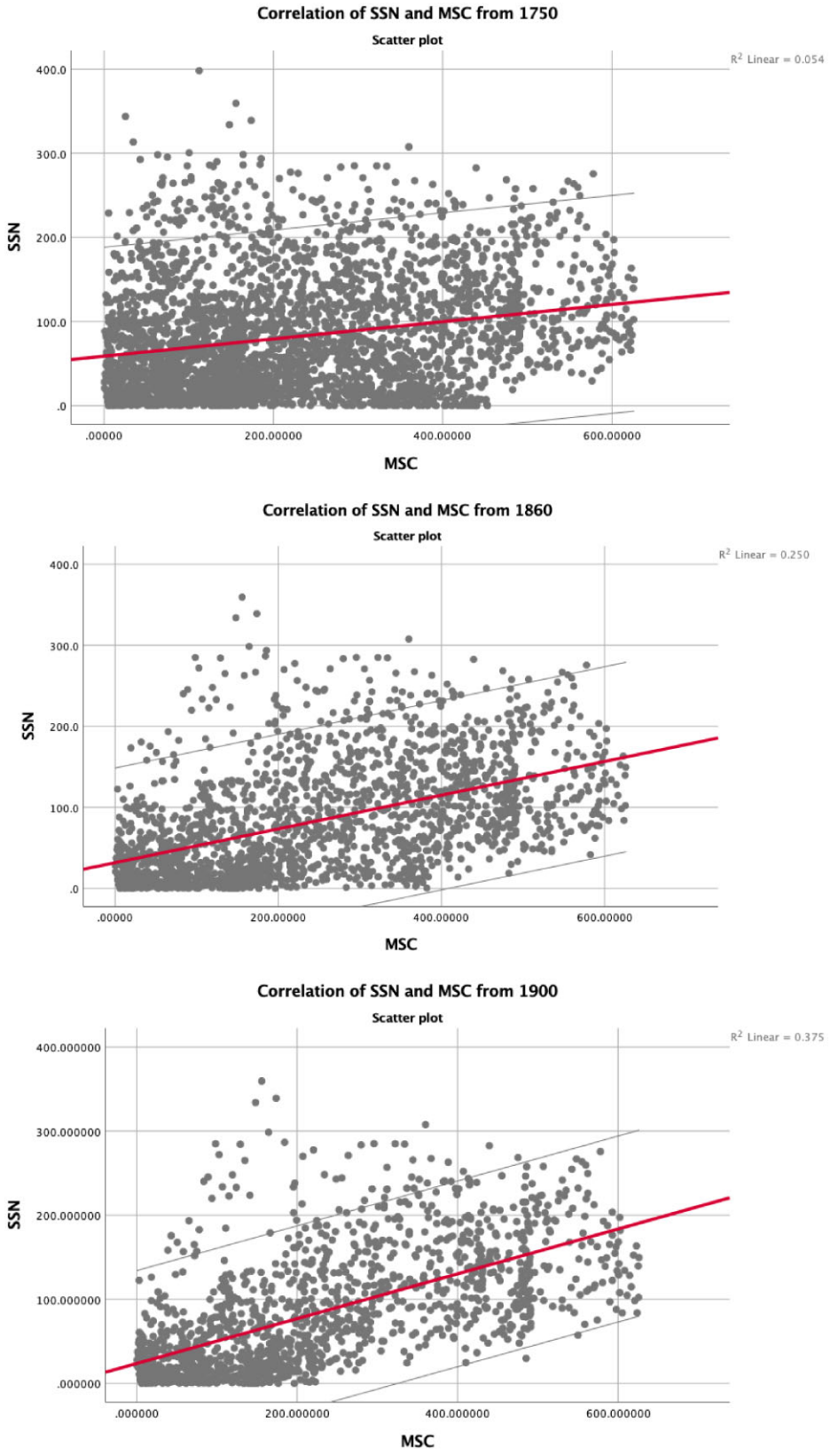

Figure 8. The scatter plots of the correlation between the averaged sunspot number SSN and MSC calculated with SPCC v28 software for different years of observations with different level of errors (see the text for details) for the observation times: from 1700 until present, Spearman correlation 0.25 (top plot), from 1860 till present, Spearman correlation 0. 56 (middle plot) and from 1900 till present, Spearman correlation 0.67 (bottom plot). In all cases the correlation is significant at the $p \leq 0.01$ level. The linear fittings of correlation curve are shown by the magenta lines; the two lines above and below the fitting lines show the 95 per cent confidence intervals.

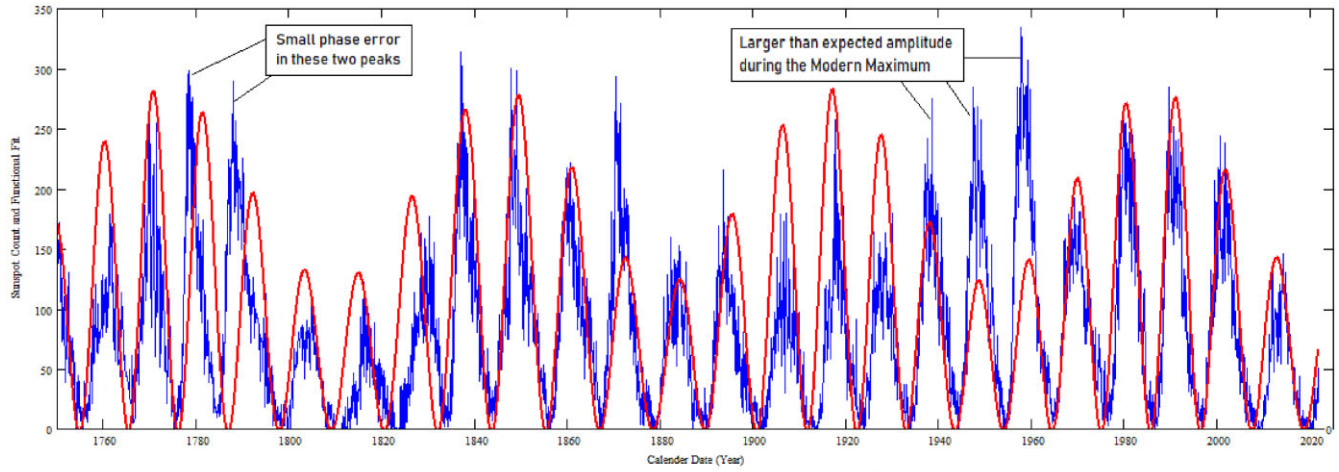

Figure 9. Fitting with the regression approach of the MSC (Shepherd et al. 2014; Zharkova et al. 2015) to the amplitudes of the averaged sunspot numbers. The sunspot numbers (SILSO World Data Center 2021) are plotted by the blue lines, the MSC curve presented by the red lines.

the times of maxima. However, it fails for fit the exact magnitudes of maxima of 11 yr cycles in MSCs and does not show the correct dates and cycle magnitudes for Maunder minimum or the modern GSM.

While, if we leave the parameters of the eigenvectors of the SBMF as they are derived from the PCA and Hamiltonian approach (Zharkova et al. 2015), the timings of the both GSMs become correct, while the amplitudes or positions of the individual cycles do not fit to the maximum amplitudes in many cycles and some positions of these maxima in sunspot cycles in SSN seen in the early years. This outcome makes us think that besides the uncertainties in timing of some early observations in 18th–mid-19th centuries cannot be the only reason for the discrepancies. The errors are not only coming from a poor coverage of sunspot detection in the early years but should also have more systematic reasons for discrepancies coming from the different entities, which these two curves represent: toroidal magnetic field for SSN and poloidal magnetic field for MSC.

Keeping in mind that the summary curve represents the two principal eigenvectors of the SBMF while the SSN series represents some sort of toroidal field but not exactly the magnetic field as they include numbers of sunspots but not their areas, which are proportional to magnetic fields. This difference between the properties of the series of SSN and MSC can explain the difference in the amplitudes of cycles −2 to 4 in the time interval closer to Maunder minimum where the amplitudes of poloidal field, or MSC, are much lower than that of SSN and for cycles 9–17 where the poloidal magnetic field, or MSC, magnitudes were much higher.

In addition to any observational restrictions of deriving the SSN curve discussed in Section 2.3.2, these differences between the MSC and SSN cycles could also indicate a real difference between the features produced on the solar surface by poloidal and toroidal magnetic fields during these periods. These differences can be linked to some specific interaction of two magnetic fields in the solar dynamo model as discussed later in Section 3.3.3.

3.3 Possible reasons for discrepancies between SSN cycles and MSC

There could be a few reasons of the different appearances of SSN and MSC: a poor coverage of the observations during early years, uncertainties with times of observations in the 19th century related to calendar migration as discussed in Section 3.3.1, some uncertainties in reproducing SSN with only two eigenvectors (and MSC) generated only by dipole magnetic sources discussed in Section 3.3.2 and the real differences expected between representation on the solar surface of different solar magnetic entities: toroidal and poloidal magnetic fields as discussed in Section 3.3.3.

3.3.1 Uncertainties in the early observations of SSN

This discrepancies between SSN and MSC representations in the 18th–19th centuries demonstrated by the shifts of the MSC cycle maxima by 5–6 yr form SSN can be explained by a lack of observations in the period of 1720–1760 (see Fig. 1, bottom plot) and/or by unreliable dating of the observations in other periods of the 19th century, especially in 1830–1860. The latter can be caused by variable migration times from the Julian to Gregorian calendars in different countries and by the other problems discussed in Sections 2.1 and 2.3.2.

The contribution to these problems can be mixed not only with the physical absence of observations but also with a big misunderstanding in the dating accurately of sunspot drawings because of the calendar change from Julian to Gregorian at different times in different countries, or with the varying starts of New Years in different countries that could also make a complete mess in shifting the dates assigned for the sunspots by more than a year.

This is partially verified by the recent restorations of SSN from the other than sunspot definitions, e.g. from the isotope abundances (Usoskin et al. 2021) and Bayesian approach (Velasco Herrera et al. 2021, 2022) shown in Fig. 7, where some early maxima were shifted closer to the MSC positions. Although there is no other way to prove the real position of sunspots in 18th–19th centuries unless new trustworthy sources of sunspot drawings are found.

3.3.2 Representation of solar activity with MSC of two principal components

There is also a possibility of some uncertainty in the detected two eigenvalues and vectors of the observed SBMF used for PCA (Zharkova et al. 2012; Zharkova et al. 2015), which are the observational facts dependent on the accuracy of a magnetic field detection and their representation by series of periodic functions.

The accuracy of representation of the two eigenvectors by the series with five cosine functions was evaluated earlier to be not lower that 97 per cent (Shepherd et al. 2014; Zharkova et al. 2015).

The Scree's plot of the eigenvalues from the PCA [see fig. 1 in Zharkova et al. (2012); Zharkova & Shepherd (2022)] show that the eigenvalues remain the same after the extra cycle 24 is added to the PCA. The eigenvectors, indeed, come in pairs, with the first pair of PCs covering 39 per cent of the magnetic data by variance of SBMF in cycles 21–23, or 67 per cent by standard deviation (SD). These two eigenvectors, PCs, are used to build the summary curve and MSC. This meant that these two PCs, by default, can be responsible only for 67 per cent of the whole SBMF data by SD.

The most recent investigation of the eigenvectors of SBMF from cycles 21–24 (Zharkova & Shepherd 2022) has also confirmed that the addition to the data of the extra solar cycle 24 did not change the eigenvalues and eigenvectors for the first four pair, or eight eigenvectors, covering 95 per cent of the data by SD. Hence, in order to have a higher correlation between SSN and MSC, the other three pairs of eigenvectors, or magnetic waves, created by quadruple, sextuple, and octuple magnetic sources are required (Zharkova & Shepherd 2022). This is a reassuring finding, which strengthens the PCA case for using the eigenvectors of poloidal field as a proxy of solar activity, in addition to the existing solar activity index defined by the averaged sunspot numbers.

If in the future we manage to add to the summary curve the next pair of eigenvectors, assigned to quadruple magnetic sources (Popova et al. 2018), the summary curve will have four eigenvectors and can cover more than 77 per cent of the observational data by SD (Zharkova & Shepherd 2022). Therefore, the MSC index derived from the WSO magnetic field observations provide valuable information for theoreticians about the poloidal field waves detected on the solar surface, which can be directly compared with the model simulations.

3.3.3 Links to the waves of solar dynamo

Another reason of the differences between SSN and MSC can be defined by different physical entities represented by the MSC, representing poloidal magnetic field, and by sunspot index SSN representing toroidal field. The question is whether these two magnetic fields in the dynamo models, poloidal, and toroidal, have the similar or different appearances. Otherwise, the MSC and SSN curve differences can reflect the real differences between the generated toroidal (sunspots) and poloidal (SBMF) magnetic fields.

Since the observations of SBMF has shown us two waves formed in two layers, we can use these waves to derive the parameters of solar interior and dynamo model parameters required to construct the solutions of the dynamo equations (Zharkova et al. 2015) resembling the two waves derived from the two eigenvectors. There are a number of dynamo models considering simulations of the dynamo waves in two different layers (Parker 1993; Dikpati, Gilman & Ulrich 2010; Belucz, Dikpati & Forgács-Dajka 2015; Bekki & Yokoyama 2017; Pipin & Kosovichev 2018), which can be used to account for the observed magnetic waves.

We use Parker's two layers dynamo model with meridional circulation (Parker 1993), like in our previous simulations of poloidal and toroidal magnetic fields of the Sun and the dynamo parameters derived from fitting this mode to the eigenvectors, or magnetic waves, derived with PCA (see Fig. 6, top plot in Zharkova et al. 2015). The simulations revealed rather close resemblance of the simulated temporal magnetic wave variations for the poloidal field to the two eigenvectors and their summary curve derived from the two PCs for 2000 yr shown in Fig. 4 taken from Zharkova et al. (2015).

For the goal of this paper, we present in Fig. 10, top and bottom plots the poloidal and toroidal magnetic fields respectively, simulated with this dynamo model (Zharkova et al. 2015) for 2000 yr including the current grand solar cycle (GSC), lasting from MM until the modern GSM. Note that this is not the only double dynamo model, which can be used to interpret the observational eigenvectors derived from SBMF as per references above. But we used it to demonstrate that solar activity is formed by these waves, generated by dipole magnetic sources, as minimum, and/ or by other waves, generated by quadruple, sextuple, and octuple magnetic sources.

These plots visibly demonstrate that the appearance of poloidal and toroidal magnetic fields are, in fact, rather different. The amplitudes of poloidal magnetic field in the current grand solar cycle (GSC; 1685–2043) varies very significantly with time of the GSC, whereas the amplitudes of toroidal field are much less changeable during the GSC decreasing only towards GSMs. This means that the difference in amplitude of magnetic field in cycles between the SSN and MSC is real and defined by the different solar dynamo actions in different entities.

In addition to the temporal variations of poloidal magnetic field (Zharkova et al. 2015), we can also simulate the butterfly diagrams for the previous grand solar cycle including the Maunder minimum (MM; Fig. 11, top plot). It shows that the simulations off sunspots were rather sparse during 1645–1700) while appearing in the years 1700, 1710, and 1720 that fits rather closely the sunspots measured for the MM as shown in Fig. 11, top plot (Spörer 1889; Eddy 1976; Ribes & Nesme-Ribes 1993).

The model of the butterfly diagram for the current and the next grand solar cycles including the modern GSM (see Fig. 11, bottom plot) reveals the absence of sunspots in the butterfly diagram only during cycle 26, while there are some remaining magnetic activity observed during cycles 25 and 27. This indicates that the modern GSM (2020–2053) will be shorter, and the solar activity (magnetic field) will slightly higher than during MM.

This correspondence of the simulated and observed sunspots during Maunder minimum reassure us that the dynamo model parameters selected from a comparison with the observed eigenvectors work well, meaning that our understanding of the derived curves and their role in solar activity is close to reality. These simulations prove that undoubtedly, the appearances of solar activity represented by sunspots, SSN, and by SBMF, MSC, are meant to be different in the amplitude maxima and shapes at different phases of the grand solar cycles.

4 CONCLUSIONS

In the current paper, we attempted to establish a link between the solar activity index defined by averaged sunspot numbers, SSN, and a proposed proxy – a summary curve of the eigenvectors, or MSC, derived with PCA from the observed SBMF.

Tremendous work has been done by numerous researchers to setup the current solar activity index – the averaged sunspot numbers (SILSO World Data Center 2021). Schwabe (1843) discovered a frequency of occurrence of spots with a cycle to be ∼10 yr, which was later redefined to 11.1 yr (Wolf 1852), when systematic observations of sunspots were organized and the concept of a daily 'relative' sunspot number was introduced.

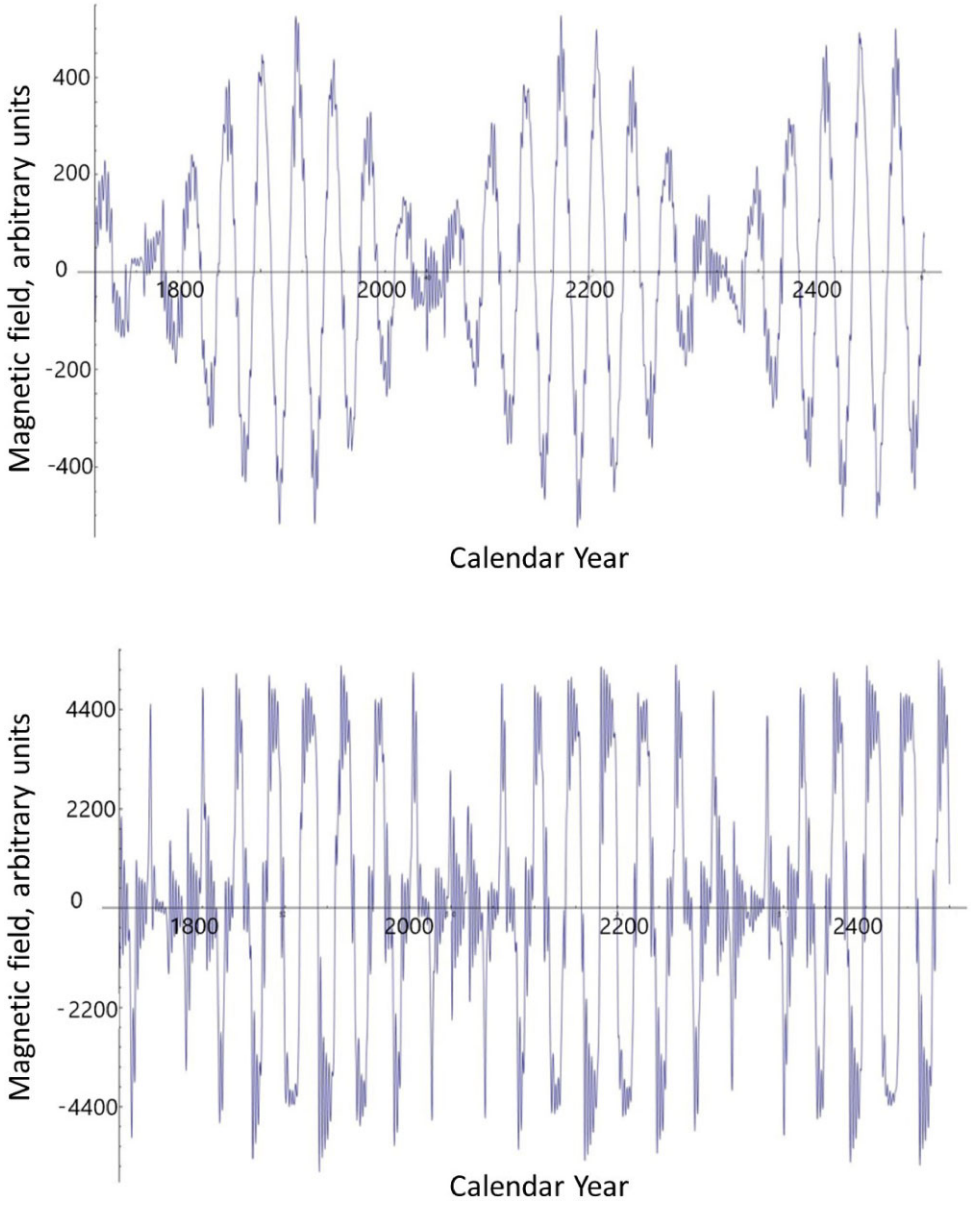

Figure 10. The simulated poloidal (top plot) and toroidal (bottom plot) magnetic fields generated by the solar dynamo for 1000 yr covering the modern grand solar cycle in the centre.

The sunspot series was revised in 1998 by Hoyt & Schatten (1998a, b) producing a revised sunspot series with sunspot groups (GSN). Later the international team of researchers reconstructed again an almost 400 yr history of sunspot activity from 1610 to the 2000s (Svalgaard & Schatten 2016, 2017a, b). They discovered that the observations of sunspots in different periods were not consistent that restricted reliability of the built sunspot numbers in the 18th century and in the first half of 19th century.

Recently the SILSO International Data Center (Sunspot Index and Long-term Solar Observations) at the Royal Observatory of Belgium revised the sunspot series with a correction of the last 30 yr of observations (Clette et al. 2014, 2015) and considered all the restorations to be slightly different from 1750 until 1900 while becoming rather agreeable after 1900 (Leussu et al. 2013; Clette et al. 2014; SS16).

Zharkova et al. (2015) suggested to use eigenvectors of SBMF derived with PCA from the synoptic magnetic maps obtained by Wilcox Solar Observatory for three (21–23) (Zharkova et al. 2012),or four cycles 21–24 (Zharkova & Shepherd 2022) and derived the first eight significant eigenvectors covering the majority of the magnetic data by variance.

The summary curve of the two PCs assigned to the magnetic waves generated by dipole magnetic sources, was suggested to be an additional solar activity index, whose modulus curve is shown linked to the averaged sunspot numbers (Shepherd et al. 2014; Zharkova et al. 2015). This summary curve of two PCs was suggested as a new proxy of solar activity as it reflects the complementary entity of solar activity – poloidal magnetic field.

The summary curve calculated backward to 1200 and forward by 1200 yr revealed very distinct variations of the cycle amplitudes in every 350–400 yr, or grand solar cycles (Zharkova et al. 2015). These

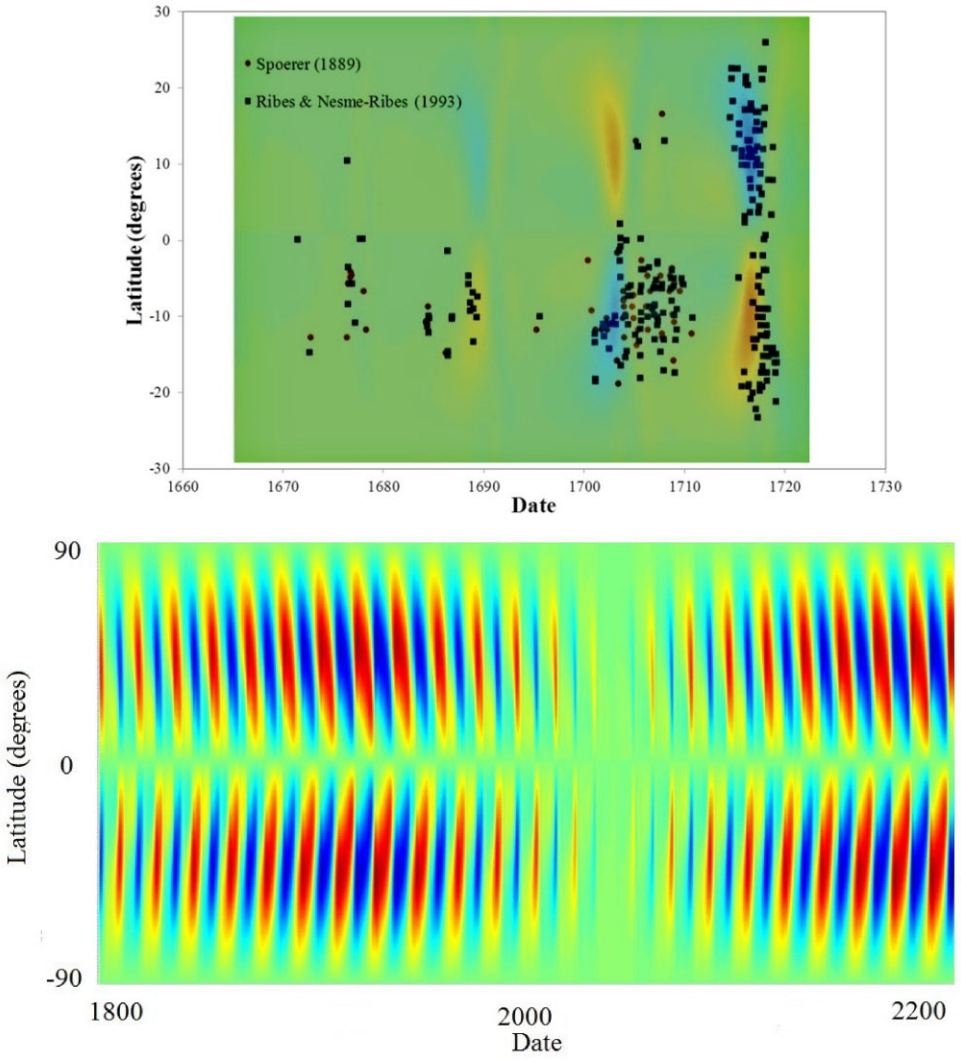

Figure 11. Top plot: The butterfly diagrams derived from the observations of Maunder minimum (top plot) (the dots are taken from Spörer 1889; Ribes & Nesme-Ribes 1993) overlaid with the butterfly diagram (light blue and yellow colours show the opposite leading polarities of toroidal field) simulated with the two layers dynamo model with meridional circulation using the dynamo parameters derived from the two eigenvectors (Zharkova et al. 2015). Bottom plot: The butterfly diagram simulated using the same dynamo model (red and navy colours show the opposite leading polarities of toroidal field) for the current and next grand solar cycles in years 1800–2200 including the modern GSM (2020–2053) between them (Zharkova et al. 2015).

grand solar cycles are separated by GSMs, when the amplitudes of 11 yr cycles become very small, similar to those reported in Maunder, Wolf, Oort, and other GSMs. It turned out that there is a steady decrease of the cycle amplitudes from cycles 21–24 entering into the modern GSM (2020–2053).

Recently, solar activity indices were restored with Bayesian models and used to predict solar activity for next few solar cycles (VH21) as well as extending their model for a description of the whole set of sunspot index d including Maunder minimum (Velasco Herrera et al. 2022). The Bayesian fitting have shown some problems for the full SSN data set, which either fitting the Maunder minimum but missing the modern GSM in cycles 25–27 (Zharkova et al. 2015) or fitting the modern GSM with Bayesian restoration if the sunspot data taken after 1900. This highlights importance of estimation of the data uncertainties in SSN in the early observation in the 18th–19th centuries.

In the current paper, a direct comparison was made between MSC and the whole data set of sunspot cycle indices SSN since 1700, by applying wavelet and Fourier spectral analysis of both data sets and by performing correlation analysis with the SPSS for the periods from 1700, 1860, and 1900 until present.

We established that both series have a rather close correspondence of the timings, duration, and maxima times in cycles from 12 to 24, 6, 7, and −4, −3. Although, the distribution of sunspot cycles in the 18th century when some SSN cycles had durations of 7 or 8 yr while others lasted for 15 yr while the MSC curve reveals pretty regular cycles. Some MSC cycles show double maxima (cycles 1–4) or triple maxima (Ψ-type) distributions in cycles 0 and 1 and cycles −1 and −2 before MSC and SSN come into Maunder minimum. The MSC cycles closer to 1700–1750 reveal smaller maximal magnitudes (cycles −3 to 0 and 1–4) than the amplitudes of sunspot index, while cycles −2 to 0 have reversed maxima with minima in SSN and MSC curves.

The wavelet and Fourier spectra of SSN and MSC series reveal the most prominent periods to be the same one of 10.7 yr within 95 per cent confidence interval, while SSN series shows confidently

an additional period of 101 yr and MSC series a period of 342 yr. These periods are detected well above the red noise level clearly indicated in the spectral analysis. There is also a weak indication at the border of the 95 per cent confidence level of the period of 60.6 yr in both sunspots and MSC, and of some other periods occurring below this confidence level. The absence of centennial period of 101 yr in the MSC is explained by the absence of the second pair of eigenvectors in the MSC, reflecting quadruple magnetic waves, which are shown to contribute to centennial oscillations (Gleisberg cycle; Popova et al. 2018). While the absence of period of 342 yr in sunspot data can be explained by a short time-scale of SSN of 320 yr, which cannot detect, by default, a larger period of 342 yr.

Correlation analysis between the SSN and MSC series using both Pearson (for normal distributions) and Spearman correlation (for other distributions) with SPSS package established that the correlation coefficients vary from 0.25 for the whole SSN data set (from 1700 till present), to 0.56 from the data sets from 1860 and 0.67 for the data sets from 1900 when all the restorations of the SSN are agreed. This confirms that the SSN and MSC data sets are closely related as they should be representing the solar activity in different entities of the action of solar dynamo, toroidal (SSN), and poloidal (MSC) magnetic fields.

Therefore, the discrepancies occurring between the data sets can be partially explained by (i) poor, or lack of, sunspot observations or (ii) a difference of the magnetic field entities (poloidal for MSC versus toroidal for SSN magnetic field). The first reason can include the absence of observations, a mixture with the dates of sunspot drawings induced by changes from Julian to Gregorian calendars made at different times in different countries or even by a mix in the year number because of different starts of New Years in some counties. It is rather difficult to know, which of these reasons contribute; although, recent evaluation of solar cycle maxima times from the carbon 14 isotopes lent some support to the MSC times of maxima in early observations by shifting some cycle maxima in the directions of MSC maxima.

The second reason is well understood in terms that the MSC is produced by poloidal magnetic field of the Sun while the averaged sunspot numbers are loosely associated with toroidal magnetic field, though this link is rather distant via the number of sunspots in groups. The appearance differences in toroidal and poloidal fields *i* for a given grand solar cycle are clearly demonstrated in the simulations carried for the two layer dynamo model with meridional circulations, which successfully explained the observed summary curve for the current grand solar cycle, butterfly diagrams for the Maunder minimum and predicted the periods of sunspot activity in butterfly diagrams for the modern GSM.

Of course, the PCA and mathematical description of eigenvectors can introduce some errors into the predicted eigenvectors and their summary curve, which is suggested as am additional proxy for the solar activity index. However, the most recent investigation of eigenvectors of SBMF from cycles 21–24 (Zharkova & Shepherd 2022) has revealed that the addition of the magnetic field data from the extra solar cycle 24 did not change the eigenvalues and eigenvectors, at least, for the first four pairs, or eight eigenvectors. This is reassuring finding, which helps to consider the eigenvectors of poloidal field, or their MSC, as a proxy of solar activity, in addition to the existing solar index defined by averaged sunspot numbers SSN.

A usage of these two indices, averaged sunspot numbers SSN and MSC of eigenvectors, which now become also available as an supplementary array for 2000 yr, can pour a light into the solar activity long-term evolution from two different perspectives: toroidal magnetic field of sunspots and poloidal magnetic field of SBMF. This second proxy of solar activity would be a very useful addition, in general, and timely addition, specifically, as the index capable to explain long-term solar activity including GSMs caused by the magnetic wave interference.

ACKNOWLEDGEMENTS

The authors wish to express their deepest gratitude to the two anonymous reviewers for useful and constructive comments, from which the paper strongly benefited. The authors would like to thank the Solar Influences Data Analysis Center (SIDC) at the Royal Observatory of Belgium for providing the corrected averaged sunspot numbers. The authors also express their deepest gratitude to the staff and directorate of Wilcox Solar Observatory for providing the coherent long-term observations of full disk synoptic maps of the solar background magnetic field. The authors are very grateful to Mr R. Barnard for his great help with the historic input about the British calendar, valuable language and style editions, and discussion of the paper results.

DATA AVAILABILITY STATEMENT

The data underlying this article will be shared on reasonable request to the corresponding author.

REFERENCES

Arlt R., 2008, Sol. Phys., 247, 399
Arlt R., 2009, Sol. Phys., 255, 143
Arlt R., Vaquero J. M., 2020, Living Rev. Sol. Phys., 17, 1
Arlt R., Senthamizh Pavai V., Schmiel C., Spada F., 2016, A&A, 595, A104
Beer J., Tobias S., Weiss N., 1998, Sol. Phys., 181, 237
Bekki Y., Yokoyama T., 2017, ApJ, 835, 9
Belucz B., Dikpati M., Forgács-Dajka E., 2015, ApJ, 806, 169
Cameron R. H., Schüssler M., 2013, A&A, 557, A83
Cameron R. H., Schüssler M., 2019, A&A, 625, A28
Carrasco V. M. S., Vaquero J. M., Trigo R. M., Gallego M. C., 2018, Sol. Phys., 293, 104
Carrasco V. M. S., Gallego M. C., Vaquero J. M., 2020, MNRAS, 496, 2482
Carrasco V. M. S., Gallego M. C., Villalba Álvarez J., Vaquero J. M., 2021, Sol. Phys., 296, 59
Chatzistergos T., Usoskin I. G., Kovaltsov G. A., Krivova N. A., Solanki S. K., 2017, A&A, 602, A69
Clette F., Svalgaard L., Vaquero J. M., Cliver E. W., 2014, Space Sci. Rev., 186, 35
Clette F., Svalgaard L., Vaquero J. M., Cliver E. W., 2015, The Solar Activity Cycle, Space Sciences Series of ISSI, Vol. 53. Springer Science+Business Media, New York, p. 35
Cliver E. W., 2016, Sol. Phys., 291, 2891
Courtillot V., Lopes F., Le Mouël J. L., 2021, Sol. Phys., 296, 21
Dikpati M., Gilman P. A., Ulrich R. K., 2010, ApJ, 722, 774
Dreyer J. L. E., 1903, Observatory, 26, 461
Eddy J. A., 1976, Science, 192, 1189
Hathaway D. H., 2013, Sol. Phys., 286, 347
Hathaway D. H., 2015, Living Rev. Sol. Phys., 12, 4
Hathaway D. H., Wilson R. M., Reichmann E. J., 2002, Sol. Phys., 211, 357
Hayakawa H., Tamazawa H., Ebihara Y., Miyahara H., Kawamura A. D., Aoyama T., Isobe H., 2017, PASJ, 69, 65
Hayakawa H., Kuroyanagi C., Carrasco V. M. S., Uneme S., Besser B. P., Sôma M., Imada S., 2021, ApJ, 909, 166
Hoyt D. V., Schatten K. H., 1998a, Sol. Phys., 179, 189
Hoyt D. V., Schatten K. H., 1998b, Sol. Phys., 181, 491
Hoyt D. V., Schatten K. H., Nesme-Ribes E., 1994, Geophys. Res. Lett., 21, 2067

Kane R. P., 2008, Sol. Phys., 248, 203
Karoff C., Jørgensen C. S., Senthamizh Pavai V., Arlt R., 2019, Sol. Phys., 294, 78
Kitiashvili I. N., 2020, ApJ, 890, 36
Le Mouël J.-L., Lopes F., Courtillot V., 2017, Sol. Phys., 292, 43
Leussu R., Usoskin I. G., Arlt R., Mursula K., 2013, A&A, 559, A28
Livingston W., Penn M. J., Svalgaard L., 2012, ApJ, 757, L8
Lockwood M., Owens M. J., Barnard L., 2014, J. Geophys. Res. (Space Phys.), 119, 5183
Lockwood M., Owens M. J., Barnard L., 2016, Sol. Phys., 291, 2843
Maunder E. W., 1922, J. Brit. Astron. Assoc., 32, 140
Muñoz-Jaramillo A., Vaquero J. M., 2019, Nat. Astron., 3, 205
Nagovitsyn Y. A., Pevtsov A. A., Livingston W. C., 2012, ApJ, 758, L20
Neuhäuser R., Arlt R., Richter S., 2018, Astron. Nachr., 339, 219
Newitt L. R., Dawson E., 1984, Geophys. J., 78, 277
Newitt L., Mandea M., McKee L., Orgeval J.-J., 2002, EOS Trans., 83, 381
Obridko V. N., Sokoloff D. D., Pipin V. V., Shibalvaa A. S., Livshits I. M., 2021, MNRAS, 504, 4990
Ogurtsov M. G., 2013, Geomagn. Aeronomy, 53, 663
Parker E. N., 1955, ApJ, 122, 293
Parker E. N., 1993, ApJ, 408, 707
Pipin V. V., Kosovichev A. G., 2018, ApJ, 854, 67
Popova E., Zharkova V., Zharkov S., 2013, Ann. Geophys., 31, 2023
Popova E., Zharkova V., Shepherd S., Zharkov S., 2018, J. Atmos. Sol.-Terr. Phys., 176, 61
Ribes J. C., Nesme-Ribes E., 1993, A&A, 276, 549
SILSO World Data Center, 2021, WDC-SILCO. Royal Observatory of Belgium, Brussels, available at https://wwwbis.sidc.be/silso/datafiles
Schmidt M., Lipson H., 2009, Science, 324, 81
Schove D. J., 1983, Sunspot Cycles, Hutchinson Ross Publishing Co., Stroudsburg, PA, 410
Schwabe M., 1843, Astron. Nachr., 20, 283
Shepherd S. J., Zharkov S. I., Zharkova V. V., 2014, ApJ, 795, 46
Simpson J., 2020, J. Brit. Astron. Assoc., 130, 15
Solanki S. K., Usoskin I. G., Kromer B., Schüssler M., Beer J., 2004, Nature, 431, 1084
Soon W. W.-H., Yaskell S. H., 2003, The Maunder Minimum and the Variable Sun-Earth Connection. World Scientific Publishing Co. Pte. Ltd.
Spörer G. F. W., 1889, Ueber die periodicität er sonnenflecken seit dem jahre 1618: vornehmlich in bezug auf die heliographische breite derselben, und nachweis einer erheblichen störung dieser periodicität während eines langen zeitraumes.... Vol. 53. Blochmann, Germany
Stix M., 1976, A&A, 47, 243
Svalgaard L., 2017, Sol. Phys., 292, 4
Svalgaard L., Schatten K. H., 2016, Sol. Phys., 291, 2653
Svalgaard L., Schatten K. H., 2017a, preprint (arXiv:1704.07061)
Svalgaard L., Schatten K. H., 2017b, preprint (arXiv:1705.02024)
Svalgaard L., Schatten K. H., 2017c, preprint (arXiv:1706.01154)
Tamazawa H., Kawamura A. D., Hayakawa H., Tsukamoto A., Isobe H., Ebihara Y., 2017, PASJ, 69, 22
Torrence C., Compo G. P., 1998, Bull. Am. Meteor. Soc., 79, 61
Usoskin I. G., Mursula K., Solanki S., Schüssler M., Alanko K., 2004, A&A, 413, 745
Usoskin I. G., Solanki S. K., Krivova N. A., Hofer B., Kovaltsov G. A., Wacker L., Brehm N., Kromer B., 2021, A&A, 649, A141
Vaquero J. M., 2007, Adv. Space Res., 40, 929
Vaquero J. M., Gallego M. C., 2014, Adv. Space Res., 53, 1162
Vaquero J. M., Gallego M. C., Trigo R. M., 2007, Adv. Space Res., 40, 1895
Vasilieva I., Zharkova V., 2022, preprint (arXiv:2203.03637)
Vasiljeva I. E., Pishkalo M. I., 2021, Kinemat. Phys. Celest. Bodies, 37, 200
Velasco Herrera V. M., Soon W., Legates D. R., 2021, Adv. Space Res., 68, 1485
Velasco Herrera V. M., Soon W., Hoyt D. V., Murakzy J., 2022, Sol. Phys., 297, 8
Vokhmyanin M., Arlt R., Zolotova N., 2021, Sol. Phys., 296, 4
Waldmeier M., 1961, The sunspot-activity in the years 1610–1960. Schulthess, Zurich
Willamo T., Usoskin I. G., Kovaltsov G. A., 2017, A&A, 601, A109
Wolf R., 1850a, Astron. Mitt. Eidgenöss. Sternwarte Zur., 1, 3
Wolf R., 1850b, Astron. Mitt. Eidgenöss. Sternwarte Zur., 1, 15
Wolf M., 1852, MNRAS, 13, 29
Wolf R., 1877, Geschichte der astronomie. R. Oldenbourg, Munchen
Zhao J., Bogart R. S., Kosovichev A. G., Duvall T. L., Jr, Hartlep T., 2013, ApJ, 774, L29
Zharkov S., Gavryuseva E., Zharkova V., 2008, Sol. Phys., 248, 339
Zharkova V., 2020, Temperature, 7, 217
Zharkova V. V., Shepherd S. J., 2022, MNRAS, 512, 5085
Zharkova V. V., Shepherd S. J., Zharkov S. I., 2012, MNRAS, 424, 2943
Zharkova V. V., Shepherd S. J., Popova E., Zharkov S. I., 2015, Nat. Sci. Rep., 5, 15689
Zharkova V. V., Shepherd S. J., Popova E., Zharkov S. I., 2018a, J. Atmos. Sol. -Terr. Phys., 176, 72
Zharkova V. V., Shepherd S. J., Popova E., Zharkov S. I., 2018b, in Foullon C., Malandraki O. E., eds, Proc. IAU Symp. 335, Space Weather of the Heliosphere: Processes and Forecasts, p. 211
Zito R. R., 2016, Sociol. Anthropol., 4, 953

This paper has been typeset from a TEX/LATEX file prepared by the author.